Tracking viral genomes in host cells at single-molecule resolution

Wang, I-Hsuan ; Suomalainen, Maarit ; Andriasyan, Vardan ; Kilcher, Samuel ; Mercer, Jason ; Neef, Anne ; Luedtke, Nathan W ; Greber, Urs F

Abstract: Viral DNA trafficking in cells has large impacts on physiology and disease development. Current methods lack the resolution and accuracy to visualize and quantify viral DNA trafficking at single-molecule resolution. We developed a noninvasive protocol for accurate quantification of viral DNA-genome (vDNA) trafficking in single cells. Ethynyl-modified nucleosides were used to metabolically label newly synthesized adenovirus, herpes virus, and vaccinia virus vDNA, without affecting infectivity. Superresolution microscopy and copper(I)-catalyzed azide-alkyne cycloaddition (click) reactions allowed visualization of infection at single vDNA resolution within mammalian cells. Analysis of adenovirus infection revealed that a large pool of capsid-free vDNA accumulated in the cytosol upon virus uncoating, indicating that nuclear import of incoming vDNA is a bottleneck. The method described here is applicable for the entire replication cycle of DNA viruses and offers opportunities to localize cellular and viral effector machineries on newly replicated viral DNA, or innate immune sensors on cytoplasmic viral DNA.

DOI: https://doi.org/10.1016/j.chom.2013.09.004

Tracking viral genomes in host cells at single molecule resolution

I-Hsuan Wang[1,2], Maarit Suomalainen[1], Vardan Andriasyan[1], Samuel Kilcher[3], Jason Mercer[3], Anne Neef[4], Nathan W. Luedtke[4] & Urs F. Greber[1,5]

[1] Institute of Molecular Life Sciences, University of Zürich, CH-8057 Zurich, Switzerland

[2] Molecular Life Sciences Graduate School, ETH and University of Zürich, CH-8057 Zurich, Switzerland

[3] Institute of Biochemistry, ETH Zurich, 8093 Zürich, Switzerland

[4] Institute of Organic Chemistry, University of Zürich, CH-8057 Zurich, Switzerland

[5] corresponding author: E-mail: urs.greber@imls.uzh.ch, Telephone: +41 44 635 48 41, Fax: +41 44 635 68 17

Running title:

Tracking single virus genomes during infection

Keywords:

Fluorescence microscopy; virus entry; virus uncoating; nuclear import; foreign DNA; trafficking; cytosolic DNA; adenovirus; vaccinia virus; herpes virus

Summary

Viral DNA trafficking in cells has large impacts on physiology and disease development. Current methods lack the resolution and accuracy to visualize and quantify viral DNA trafficking at single molecule resolution. We developed a non-invasive protocol for accurate quantification of viral DNA-genome (vDNA) trafficking in single cells. Ethynyl-modified nucleosides were used to metabolically label newly synthesized adenovirus, herpes virus and vaccinia virus vDNA, without affecting infectivity. Super-resolution microscopy and copper(I)-catalyzed azide–alkyne cycloaddition (click) reactions allowed visualization of infection at single vDNA resolution within mammalian cells. Analysis of adenovirus infection revealed a large pool of capsid-free vDNA accumulated in the cytosol upon virus uncoating, indicating that nuclear import of incoming vDNA is a bottleneck. The method described here is applicable for the entire replication cycle of DNA-viruses and offers opportunities to localize cellular and viral effector machineries on newly replicated viral DNA, or innate immune sensors on cytoplasmic viral DNA.

Highlights

1) Modified nucleoside labelling for fluorescence tracking of single virus DNA-genomes
2) Method successfully used to visualize adeno-, herpes- and vaccinia virus DNA-genomes
3) Adenoviruses expose but do not uncoat vDNA till nuclear pore complex (NPC) binding
4) Misdelivery of capsid-free adenovirus DNA to the cytosol upon uncoating at NPC

Introduction

How invading DNA traffics in cells, and triggers or avoids cytoplasmic DNA sensors, is poorly understood, largely because the tools to track and quantitate non-nuclear DNA in cells have been limited. For instance, DNA labeled with radioactive nucleoside analogues lacks critical histological and cell biological resolution and is difficult to combine with immunocytochemistry. Similarly, in situ hybridization or DNA-specific antibody labeling protocols are poorly compatible with immunocytochemistry, as they require substantial sample processing, and frequently destroy antigenicity. The same problems can be encountered when using locked nucleic acid probes or molecular beacons, since the output is strongly dependent on probe accessibility and affinity to the target DNA. These procedures are prone to false positive signals, for example by proteins binding to the beacon and leading to dequenching of fluorescence independent of target DNA (Tan et al., 2004). Likewise, binding of synthetic nucleic acids, so called aptamers, to chemical or biological targets can be used to detect DNA, albeit with similar limitations as molecular beacons (Leung et al., 2012).

In contrast to antibody- and oligonucleotide-based detection methods for DNA, metabolic labeling of DNA with “clickable” nucleoside analogues and copper(I)-catalyzed azide-alkyne cycloaddition (click, Kolb et al., 2001) reactions allows DNA visualization without sample denaturation. For example, the deoxythymidine analog 5-ethynyl-2'-deoxyuridine (EdU) has been used for DNA labeling and cell cycle studies in cells and whole organisms (Salic and Mitchison, 2008), albeit with some toxicity issues (Gierlich et al., 2006). Optimized nucleoside analogues, such as (2'S)-2'-deoxy-2'fluoro-5-ethynyluridine (F-*ara*-EdU) proved to be less toxic and allowed the identification of quiescent and senescent cells during embryogenesis.(Neef and Luedtke, 2011). Besides EdU and F-*ara*-EdU, two other alkyne-containing nucleoside analogues have been reported for DNA labeling, deoxy-5-ethynylcytidine (EdC, Guan et al., 2011; Qu et al., 2011) and 7-deaza-7-ethynyl-2’-deoxyadenosine (EdA, Neef et al., 2012). Such nucleosides have been used to study cell proliferation and differentiation, chromatin structure, and DNA damage and repair (Lu et al., 2010).

Adenoviruses and herpes viruses are DNA viruses that deliver their genomes to the nucleus (Puntener and Greber, 2009). In contrast, the poxvirus vaccinia replicates in the cytoplasm. Here we used ethynyl-modified nucleosides to metabolically label newly synthesized adenovirus, herpes virus and vaccinia virus DNA in infected mammalian cells. The labeled viral genomes could be detected by click chemistry at single viral genome sensitivity by super-resolution fluorescence microscopy or conventional confocal microscopy. Importantly, the incorporation of certain alkyne nucleosides into virions did not compromise viral infectivity, and hence the method is suitable for trafficking studies of single virus genomes.

Results

Incorporation of nucleoside analogues into adenovirus

Previous studies using non-infected cells demonstrated that EdU, EdC, F-ara-EdU and EdA were selectively incorporated into cellular DNA, giving staining that closely matched the DAPI nuclear signal (data not shown, and Guan et al., 2011; Neef and Luedtke, 2011; Neef et al., 2012; Qu et al., 2011; Salic and Mitchison, 2008). We tested if EdC, F-*ara*-EdU or EdA were incorporated into adenovirus replication centers in A549 cells infected with HAdV-C5 at multiplicity of infection (MOI) of 30. Nucleosides were added to the culture medium at 2.5 μM 4h post infection (pi). The incorporated nucleosides were detected by copper(I)-catalyzed azide-alkyne cyclo-addition reactions with Alexa-Fluor-488-Azide. Viral replication centers were visualized by an antibody directed against the adenovirus single strand-DNA binding protein (DBP) (Voelkerding and Klessig, 1986). As early as 16h pi, EdC strongly stained numerous round nuclear objects concentrically arranged around ring-like, DBP-positive structures in flower-like patterns (Fig. 1a, b). This suggested that EdC was incorporated into newly synthesized viral DNA. EdA and F-*ara*-EdU were also incorporated into viral replication domains, albeit less efficiently than EdC. At 24 h pi, however, increased amounts of EdA and F-*ara*-EdU were found in viral replication domains (Fig. 1b). We next tested if any of the nucleosides affected virus growth. At concentrations up to 5 μM, EdA and EdC or 1:1 mixtures of EdA and EdC gave the highest titers across the entire concentration range, identical to cells grown

without nucleosides, unlike F-*ara*-EdU or EdU, which gave significantly lower titers, although F-*ara*-EdU gave higher titers than EdU (Fig. 1c, d). EdC labeling of viral replication sites gave a similar pattern as fluorescence in situ hybridization (FISH) using genomic viral DNA probes (Greber et al., 1997), indicating that EdC is an authentic label for adenovirus DNA replication sites. Unlike FISH, however, EdC gave superior resolution of the replication centers (Fig. 1e). A combination of EdC and EdA at 2.5 μM was optimal for labeling nascent adenoviral DNA without affecting viral titers.

To test if the ethynyl-labeled genomes were incorporated into viruses, we grew HAdV-C5 in human bronchial epithelial A549 cells in presence of 2.5 μM EdC and EdA for 72 h, and isolated the viruses from cells by double CsCl density gradient centrifugation. Viruses were spotted on glass coverslips and analysed for EdA/EdC by staining with Alexa-Fluor-488-azide. While native viruses were not stained with Alexa-Fluor-488-azide, the heat-disrupted samples were positive for Alexa-Fluor-488-azide, and also for the capsid internal DNA-associated protein VII (VII), as indicated by fluorescence microscopy using anti-hexon staining with 9C12 as a reference for viruses (Fig. 2). The term ‘capsid’ is used here to denote fluorescent puncta stained with 9C12. This term includes entire viruses containing all capsid proteins and vDNA (extracellular particles seen in Fig. 2), partly disassembled viruses on their way to the nucleus (endosomal or cytosolic) and broken capsids after their disassembly at the nuclear pore complex (cytosolic, for review, see Puntener and Greber, 2009; Suomalainen et al., 2013; Wolfrum and Greber, 2013). The capsid signal measured in Fig. 2 was similar to fluorophore-tagged adenoviruses, which were monodisperse as concluded from electron microscopy and fluorescence microscopy profiling (Nakano and Greber, 2000; Puntener et al., 2011). We estimated that more than 90% of the hexon-positive structures were positively labeled with Alexa-Fluor-488-azide (Fig. 2). The data show that EdA/EdC containing genomes were effectively incorporated into HAdV-C5 particles at low micromolar nucleoside concentrations, whereas F-*ara*-EdU was incorporated into HAdV-C5 only at high concentration (40 μM, not shown).

Ethynyl-modified nucleosides are incorporated into Vaccinia virus and Herpes simplex virus replication sites

To determine if ethynyl-modified nucleosides could be used to label other DNA viruses, we tested if EdC, F-*ara*-EdU, EdA and EdU were incorporated into vaccinia virus (VACV) replication compartments in the cytoplasm. BSC-40 cells were pre-loaded with the ethynyl-modified nucleosides for 24 h, and infected with VACV Western Reserve (WR) strain harbouring an mCherry fusion of the core protein A4 (WR mCherry-A4, Stiefel et al., 2012) at MOI 10 for 5 h. The presence of perinuclear sites positive for mCherry-A4 and DNA (counterstained with DRAQ5) were indicative of productive VACV replication factories. While labeling infected cells with EdC weakly stained these compartments, F-*ara*-EdU or EdA gave no detectable signal of VACV replication factories, although the nucleosides were incorporated into the nuclei (Fig. 3a, DRAQ5). In contrast to F-*ara*-EdU and EdA, EdU was incorporated into both nuclei and VACV replication sites, and was found in small cytoplasmic puncta positive for mCherry-A4 (Fig. 3a, inset). The latter suggested that EdU was incorporated into VACV genomes and packaged into newly assembled virions. To test if the ethynyl-modified nucleosides affected viral titers, BSC-40 cells were incubated with EdC, F-*ara*-EdU, EdA or EdU together with VACV. Newly synthesized VACV was harvested 24 h pi, and the plaque forming units (pfu) determined. The data showed that 0.63 µM EdU or 5 µM EdA reduced virus yields by more than 10-fold, whereas EdC and F-*ara*-EdU had essentially no effect on virus production (Fig. 3b). Since only EdU efficiently labeled VACV replication factories, 1 µM of EdU was used to produce genome-labeled VACV. Purified EdU-WR-VACV mCherry-A4 particles were permeabilised and analysed on glass coverslips for EdU by staining with Alexa-Fluor-488-azide, and mCherry fluorescence (Fig. 3c). Results show that the majority of VACV particles stained positive for EdU.

We then tested if ethynyl-modified nucleosides labeled herpes simplex virus type 1 (HSV-1) replication sites in the nucleus. A549 cells were infected with recombinant HSV-1 strain C12 at MOI of 10, followed by addition of 2.5 µM EdA, EdC or F-*ara*-EdU at 1 h pi. Samples were analysed for nucleoside incorporation at 8 h pi. Infected cells were identified by staining for the immediate early protein ICP8, a single-strand DNA-binding

protein that serves as a marker for viral replication compartments. The data show that EdA and EdC gave strong signals in ICP8 positive nuclear areas, whereas F-*ara*-EdU was positive at lower levels (Fig. S1). We conclude that different ethynyl-modified nucleosides are incorporated with variable efficiencies into DNA virus replication sites. Screening a small collection of ethynyl nucleosides is a valuable step in optimizing virus genome labeling.

Tracking of incoming single virus genomes reveals capsid-free adenovirus vDNA in the cytosol

We next investigated if single adenovirus genomes could be tracked during entry into cells. EdA/EdC labeled HAdV-C5 was bound to HeLa-ATCC cells at 4°C, and synchronized entry into cells initiated by temperature shift to 37°C. DNA was tracked by Alexa-Fluor-594-azide click reactions, and viral capsids detected by anti-hexon antibody 9C12. As expected the genomes of HAdV-C5 at the cell surface were not detected by the azide-fluorophore click reaction, similar to the intact viruses on coverslip (Fig. 4a, b). At 30 min pi, when the majority of viruses were endocytosed, escaped from endosomes to the cytosol and undergone partial uncoating (Greber et al., 1993), about 75% of the particles were positive for Alexa-Fluor-594-azide, according to confocal laser scanning microscopy analyses. The fraction of particles with accessible DNA decreased to about 33% at 150 min pi, suggesting that the vDNA was either lost or became masked. Remarkably, the drop in vDNA signal from the particles was completely inhibited by treating cells with the nuclear export inhibitor leptomycin B (LMB), which blocks the attachment of cytosolic adenoviruses to the nuclear pore complex (NPC), and prevents the complete uncoating of the viral genome (Strunze et al., 2011; Strunze et al., 2005).

To better resolve the localization of the vDNA with respect to the viral capsid, we used super-resolution confocal microscopy with a continuous wave laser and gated detection in stimulated emission depletion mode (gSTED, Hell and Wichmann, 1994; Willig et al., 2007), with a 2-3 fold improvement in spatial resolution (Fig. 4c-e). Using gSTED, the historical diffraction limit to the resolution of standard fluorescence microscopy can be

bypassed. Dual color STED at 30 min pi indicated that the vDNA stained with Alexa-Fluor-488-azide nearly perfectly colocalized with the capsid signal from the 9C12 monoclonal antibody and a secondary anti-mouse IgG conjugated with Abberior STAR 440SX (Fig. 4c). At 90 min pi, however, many capsids were devoid of vDNA, and vDNA was found next to the capsids, indicating that it had separated from capsid (Fig. 4d). Remarkably, the size of the capsid by gSTED at 30 min pi was on average 121 nm (STDEV +/- 40 nm, 346 particles), as determined by pixel intensity line profiles across the capsid and the full width at half maximum (FWHM) of the fitted Gaussian profile (Fig. 4e). This result is in broad agreement with x-ray diffraction measurements, which found a capsid size of about 80 nm (Reddy et al., 2010), plus the size of primary and secondary antibodies. The vDNA in the capsid was smaller than the capsid, gSTED average 83 nm in diameter (STDEV +/- 33 nm, 346 DNA puncta), suggesting that it is surrounded by capsid. Interestingly, the free cytoplasmic vDNA had a larger area than vDNA surrounded by the capsid, 18600 nm^2 (STDEV +/- 6200 nm^2) as opposed to 14600 nm^2 (STDEV +/- 4700 nm^2) at average 30 and 90 min pi. This suggested that free vDNA is decondensed compared to capsid-associated vDNA (Fig. 4f, g). Of note, the size of both free vDNA and capsid-associated vDNA was identical at 90 and 150 min, and 30 and 90 min pi, respectively, showing that the compaction of the two DNA forms was invariable. Together the data indicate that the genome in cytosolic adenoviruses initially becomes accessible for labeling, and later on separates from the capsid as a consequence of virus uncoating at the NPC. These events lead to the appearance of cytosolic capsid-free vDNA, which is more decondensed than virus-associated vDNA.

To assess if the free and capsid-associated vDNA pools were located in the cytosol or endosomal vesicles, HeLa cells were infected with EdA/EdC-HAdV-C5, and the plasma membrane was permeabilised with Streptolysin O (SLO). SLO is a bacterial toxin, which selectively permeabilises the plasma membrane of eukaryotic cells (Walev et al., 2001). Unfixed SLO-treated cells were stained with Alexa-Fluor-594-azide, washed, fixed with PFA, and permeabilised with Triton X-100 to allow detection of the entire virus population in cells by anti-hexon antibody staining (Fig. 5a, b). Capsid-associated vDNA was scored prominently at 30 min pi, as indicated by Alexa-Fluor-594-Azide puncta colocalizing with anti-hexon puncta in the cytoplasm and near the nuclear membrane. At 90 min pi,

prominent punctate signals from free vDNA were observed in both the cytoplasm and the nucleus of SLO-treated cells, thus indicating that the free vDNA is not endosomal. In LMB-treated cells, cytoplasmic free vDNA levels were reduced, and capsid-associated vDNA enhanced. This indicated that LMB-blocked viruses contained vDNA and were located in the cytosol. To corroborate this conclusion, we controlled that the endosomes were intact in SLO- permeabilised cells. For this, we took advantage of the HAdV-C2 mutant TS1 that is defective for endosomal escape (Burckhardt and Greber, 2009; Greber et al., 1996). HAdV-C2 wild type or HAdV-C2_TS1 (TS1) do not react with the 9C12 antibody, which is specific for HAdV-C5 (see Supplemental Procedures). We could not use ethynyl-modified nucleosides to track TS1, since this virus does not uncoat (Burckhardt et al., 2011), and its genome thus would not be detectable with fluorophore-azide (see Fig. 2 and 4a). We therefore labeled TS1 with Alexa-Fluor-488, internalized the labeled TS1 viruses into HeLa cells, permeabilised the plasma membrane with SLO and perfused anti-Alexa-Fluor-488 antibodies into the semi-permeable cells. Cells were fixed, permeabilised and stained with secondary anti-rabbit IgG coupled with Alexa-594. The results showed that the majority of TS1 was inaccessible to anti-Alexa-488 antibodies in SLO-treated cells, but was readily detected by the antibody in TX-100 permeabilised cells (Fig. 5c, d).

Low efficiency nuclear import of incoming adenovirus genomes

We next addressed if click chemistry allowed the detection of incoming vDNA from EdA/EdC-HAdV-C5 in the nucleus, and tested the functionality of EdA/EdC-HAdV-C5 by FISH experiments as described earlier for HAdV-C2 (Greber et al., 1997). The results from confocal fluorescence microscopy experiments indicated that the EdA/EdC labeled vDNA was delivered to the nucleus at 150 but not 30 min pi (Fig. S2a). We therefore chose confocal fluorescence microscopy and the 150 min time point for click chemistry detection of incoming EdA/EdC-HAdV-C5 vDNA, conditions previously used to score nuclear import of vDNA-associated protein VII (Greber et al., 1997; Puntener et al., 2011; Trotman et al., 2001). Single section confocal analyses of nucleoporin-tagged cells indicated that incoming click chemistry stained vDNA and protein VII were indeed delivered across the nuclear envelope 150 min pi (Fig. S2b). The total vDNA signals and

the total vDNA delivered to the vicinity of the nucleus (defined by maximal confocal projections in and at vicinity of the nucleus) linearly correlated with the number of viruses in the range of 20-350 viruses per cell (equivalent to MOI 1 to 20, see Yakimovich et al., 2012), with R^2 values of 0.86 and 0.74, respectively (Fig. 6a, b). Similar results were obtained for nuclear targeted capsid-free vDNA, and cytoplasmic capsid-free vDNA up to 350 viruses per cell, with R^2 values of 0.58 and 0.64, respectively (Fig. S2c-e). This indicated that click chemistry reliably detected the incoming vDNA in a linear range, both within and outside the nucleus. The fraction of maximally imported nuclear vDNA was 48% with lowest values of 6% (Fig. S2f).

Similarly, the amounts of free vDNA and empty capsids had a linear correlation with the viral dose, with R^2 values of 0.82 and 0.96, respectively (Fig. 6b). This supported the notion that nuclear transport of vDNA and vDNA uncoating were not saturated in this range. Notably, the increase of empty capsids with increasing MOI was about twice as high as the increase of total free vDNA in the cell at 150 min pi, with efficiencies of 0.78 and 0.38, respectively (Fig. 6b). At 150 min pi, the ratio of vDNA puncta to hexon puncta was 73 +/- 26% (data not shown). Although empty capsids and free vDNA are 1:1 products of virus uncoating, capsid-free DNA is apparently not as efficiently detected as empty capsids, perhaps because of higher turn-over or less efficient labeling than empty capsids. It is, however, unlikely that this is due to a large fraction of empty capsids in the inoculum, since the great majority of HAdV-C5 were vDNA-positive before infection (90%, Fig. 2). The large majority (75%) of the viruses were vDNA-positive at early time points (such as 30 min pi), unlike late time points (about 17% at 150 min pi, not shown), indicating that the separation of vDNA from capsids occurred during entry and was not a property of the inoculum.

We next conservatively assessed the efficiency of nuclear import of viral genomes, and scored vDNA puncta as intra-nuclear in two central confocal sections across the nuclei, if the signals were within the DAPI region and a rim of hexon puncta known to be outside of the nucleus (Trotman et al., 2001). To ensure that any vDNA punctum was counted only once, puncta were counted only in sections where they had maximal intensity

(highlighted with white circles in Fig. S2g). We found a linear correlation over a range of 20-200 viruses per cell (R^2 = 0.57), but poor correlation above 200 viruses per cell (Fig. 6c), similar to maximal projection analyses (Fig. S2f). The maximal number of nuclear vDNA in the central sections was between 30 and 40, but most of the nuclei contained less than 15 vDNA puncta. The efficiency of overall nuclear localization of vDNA dropped from 27% at low MOI to less than 10% at high MOI of 350 viruses per cell, and the cells had less than 15% of the cell-associated vDNA in their nuclei. The data indicated that mid-section analyses of nuclear vDNA most probably underestimate and maximal projections overestimate the nuclear contents of vDNA. The true values may be somewhere in between. But regardless of the analysis, nuclear vDNA amounts poorly correlated with viral dose at high MOI, suggesting that vDNA import or retention is inefficient.

Heterogeneity of nuclear viral DNA

We further analysed the co-localization of the adenoviral DNA-associated protein VII with the vDNA. Earlier biochemical and immunological data have shown that about 800 copies of protein VII are tightly bound to vDNA in adenoviruses (Tate and Philipson, 1979; Vayda et al., 1983), and remain associated with the viral genome throughout the early phase of viral transcription in the nucleus (Chen et al., 2007; Xue et al., 2005). Furthermore, functional data have shown that protein VII associates with the immediate early viral transcriptional activator E1A and cellular chaperones, and controls early viral gene activation (Johnson et al., 2004). Accordingly, incoming protein VII has been found in the nucleus in discrete dot-like structures (Greber et al., 1997; Puntener et al., 2011; Suomalainen et al., 2013; Walkiewicz et al., 2009), but it has not been formally proven that these structures contain vDNA.

We infected HeLa cells with EdA/EdC-HAdV-C5 for 150 min and subjected the samples to click chemistry labeling with Alexa-Fluor-594-azide and co-staining with anti-VII antibodies. In agreement with earlier studies, the vast majority of protein VII puncta localized to the nucleus (Fig. 7a) (Greber et al., 1997; Puntener et al., 2011; Walkiewicz

et al., 2009). A small fraction of protein VII was found in the cytoplasm, amounting to 12.6 +/- 8.8% of the total VII, and stained positively for vDNA (Fig. 7a). In maximal projections, we found maximally 40-70 nuclear puncta of vDNA positive for protein VII, with considerable cell-cell variability (Fig. 7b, see also Fig. S2b-d).

At less than 200 viruses per cell, the nuclear localization of vDNA-associated with protein VII was dose-dependent, with R^2 = 0.57 (Fig. 7b). Accordingly, at low viral load, the nuclear vDNA was on average 83% (±16%) positive for protein VII, and the nuclear import step was not saturated. However, large cell-cell variability was observed, independent of MOI. In contrast, at high virus load (>200 particles per cell) nuclear localization of vDNA with protein VII did not correlate with virus dose (Fig. 7b). The nuclear localization of protein VII, on the other hand was viral dose-dependent from 20 to 350 viruses per cell (R^2 = 0.81, Fig. 7c), indicating that nuclear import of protein VII is not limiting. This suggests that the number of nuclear sites for vDNA but not protein VII deposition becomes limiting at high viral load. This notion was corroborated by the observation that there was more protein VII than vDNA puncta in the nucleus. Specifically, 58% (±17.4%) of the nuclear protein VII puncta in single sections were vDNA-negative, with extensive cell-cell variability, independent of MOI (not shown). Collectively, the data suggest that vDNA import into the nucleus occurs in a dose-dependent manner and thereby occupies a limited number of nuclear sites. These sites comprise both protein VII positive and negative vDNA, with the protein VII positive form being the dominant one, that is 65% +/- 18% STDEV of total nuclear vDNA from maximal projections, and 83% +/- 16% from single section assays. In addition, the nucleus harbours a significant number of discrete sites with protein VII lacking vDNA.

Discussion

Azide-alkyne ‘click’ cycloadditions provide a powerful means to address a wide variety of biological questions (Wang et al., 2012). These highly chemoselective and bioorthogonal reactions can provide high sensitivity and bioavailability at low toxicity. The chemical

modifications for clickable nucleosides, in our case an ethynyl group, introduces minimal perturbations to whole systems under study. We found that EdC, F-*ara*-EdU and EdA were integrated well by HAdV-C5, while EdU gave low viral titers throughout a 3 day replication cycle. VACV was labeled with EdU, and to a lesser extent with EdC after a 5 h infection and 24h EdU preincubation period, and HSV-1 replication sites were positive for EdC, EdA and F-*ara*-EdU at 8 h pi. This suggested that the bioavailability of the modified nucleosides did not limit the incorporation of EdC, F-*ara*-EdU, EdA or EdU, but possibly the specificity of viral nucleotide kinases and polymerases. For example, EdU reduced the growth of HAdV-C5 and VACV at low micromolar concentrations, but was incorporated into VACV DNA, although it was toxic to cells at prolonged exposure. The incorporation of EdU into VACV particles was sufficient to track the mechanism of virus uncoating (Kilcher et al., 2013). On the other hand, EdC was well tolerated by the cells, and incorporated into the replication sites of HAdV-C5, HSV-1 and VACV without reducing viral yields. EdC may thus be a starting point for developing nucleoside analogues that can be incorporated into newly synthesized vDNA but not cellular DNA, and hence would reduce toxicity and maximize anti-viral efficacy.

As exemplified by adenovirus in the present study, metabolic labeling of virus genomes in combination with click chemistry is a sensitive tool to track viral genomes at single genome resolution. The method is superior to indirect protein-based DNA tagging techniques, such as lac repressor-GFP fusion proteins binding to lac operator sequences which have to be engineered in multiple copies into the gene of interest to obtain suitable signal to noise ratios (Belmont and Straight, 1998). Furthermore, the tracking of viral genomes by click chemistry involves less perturbations than other protocols for *in situ* detection of DNA. Unlike fluorescence *in situ* hybridization (FISH, Greber et al., 1997) or bromo-deoxy-uridine (BrDU) labeling (Nguyen et al., 2010), the click chemistry procedure is fully compatible with immuno-cytochemistry of DNA-genomes. This enabled an unprecedented detailed visualization of adenovirus replication sites in the nucleus. The globular structures representing replication sites were surrounded by concentric rings of DBP and an additional layer of EdC puncta. DBP is essential for chain elongation, binds single strand DNA and drives the unwinding of double-strand DNA. The globular structures enclosed by the DBP rings are most likely made up of double-strand vDNA

associated with histones, as they have been shown to be negative for the viral DNA-associated protein V (Puntener et al., 2011). On the other hand, the DBP positive structures were weakly positive for EdC. This was similar to EM results, where BrdU nucleosides were incorporated into HAdV-C5 infected cells and labeled with immunogold (Besse and Puvion-Dutilleul, 1994). It is likely that the BrdU and EdC nucleosides in DNA associated with DBP were not well accessible to the labeling reagents. This is supported by the notion that one DBP covers approximately 7 nucleotides forming multimeric chains on the DNA and protecting it against DNAse (Nass and Frenkel, 1980; van der Vliet et al., 1978).

Incoming HAdV-C2/C5 particles undergo stepwise disassembly during their journey from the plasma membrane to the nucleus (Greber et al., 1993). Following clathrin-mediated endocytosis, viruses penetrate into the cytoplasm from early endosomes (Gastaldelli et al., 2008). Cytoplasmic viruses are morphologically intact although they have lost a number of proteins, for example fibers, proteins IIIa, IV (penton base) and VI (Burckhardt et al., 2011; Greber et al., 1993; Nakano et al., 2000). They traffic on microtubules to the nucleus by binding to dynein intermediate chain, and use dynactin to enhance both speed and extent of these motions (Bremner et al., 2009; Engelke et al., 2011). Cytosolic capsids dock to the NPC and separate their DNA from the capsid by a disruption process triggered by kinesin-1 (Strunze et al., 2011).

One noticeable finding in our study was that a significant fraction of the incoming viral genomes (~ 25%, ±13%, with considerable cell-to-cell variability) was misdelivered to the cytosol, and hence was most likely not infectious. This was unexpected, since a large fraction of the particle to pfu ratio for adenovirus is due to low efficiency of plaque formation (Greber et al., 1993; Yakimovich et al., 2012). The appearance of cytosolic vDNA was a consequence of virus docking and disassembly at the NPC, since it was completely sensitive to LMB, which precludes virus docking to the NPC and DNA uncoating (Strunze et al., 2011; Strunze et al., 2005). It is unknown if vDNA misdelivery is due to an anti-viral response at the NPC, or related to the nature of the vDNA cargo. Super-resolution microscopy showed that the cytoplasmic capsid-free vDNA was spread

out over a larger area than the capsid-associated vDNA, thus suggesting that it is unwound after being released from the capsid. We expect that the direct visualization of cytosolic viral DNA will advance the understanding of innate anti-viral mechanisms in professional antigen-presenting cells subject to viral invasion through distinct mechanisms (Mercer and Greber, 2013).

The EdA/EdC-labeled HAdV-C5 enabled us to estimate the nuclear import efficiency of the incoming viral genome. Surprisingly, a rather small fraction of incoming vDNA, maximally 6-48% (depending on MOI, and cell-cell variability), appeared to be imported into the nucleus. The localization of vDNA in the nucleus was measured by two independent assays, one analyzing confocal microscopy sections through the middle of the nucleus, and the other one scoring vDNA in the nuclear area in maximum confocal projections in z-direction. The 6-48% import efficiency was estimated from the maximum confocal projections, and is most likely an overestimation, since a fraction of the protein VII-positive, hexon-negative nuclear vDNA puncta can also be on the cytoplasmic side of the nuclear envelope. Interestingly, the number of protein VII positive nuclear vDNA puncta correlated linearly with the input virus only at low MOIs, but saturation was observed with MOIs > 200 virus particles per cell. When the number of nuclear vDNA puncta was estimated from the confocal sections through the middle of the nucleus, the number ranged from 2 to about 40 (3-28% of the total cell associated vDNA), and again saturation was observed at MOI ~ 200. Thus, the overall efficiency of nuclear import was lower at high MOI, especially above 200 viruses per cell. Since the amounts of capsid-free vDNA in and around the nucleus correlated well with virus dose, this suggested that import or localization of vDNA in subnuclear sites is limiting.

Remarkably, in contrast to vDNA, the nuclear import of protein VII was strictly dose-dependent. Protein VII is vDNA-associated and wraps-up capsid DNA in a manner similar to core histones (for a review, see Puntener and Greber, 2009). On average, there were more nuclear puncta of protein VII than vDNA, and some of them were lacking vDNA. It is possible, but unlikely that a fraction of protein VII is imported into the nucleus independently of vDNA. More likely is that protein VII separates from vDNA in

the nucleus, or that a fraction of vDNA is modified such that the ethynyl-groups can no longer be labeled with the azide.

The fate of incoming protein VII is controversial. The number of protein VII puncta in the nucleus has been shown to be stable until around 10 h pi depending on DNA transcription and E1A expression, but not DNA replication (Chen et al., 2007). Similar conclusions were derived from chromatin immuno-precipitation experiments showing that both protein VII and histone 3 were associated with E1A/E3/E4 promoter regions (Komatsu et al., 2011). These results suggest that protein VII stays attached to the viral genome throughout early infection. Another study, however, found that a significant fraction of protein VII was degraded within a few hours of infection independent of MOI in the range of 50-500, as analysed by Western blotting (Ross et al., 2011). Within 6 h, the incoming DNA showed physiologically spaced nucleosome-like structures. Regardless of the mechanism by which protein VII separates from vDNA, our data suggest the possibility that a fraction of protein VII functions in the nucleus independently of the vDNA. By analogy to the NS1 protein of H3N2 influenza virus, which has a histone-like sequence and suppresses the expression of antiviral genes (Marazzi et al., 2012), protein VII could affect the epigenetic circuits of the host cell during the early phase of the infection. Together with a report that EdU was incorporated into pseudo-particles of human papillomavirus 16 (Lipovsky et al., 2013), our results strongly suggest that click chemistry is a general tool to track the genomes of DNA-viruses.

Experimental Procedures

Adenovirus and VACV labeled with clickable nucleosides

Adenoviruses were grown, isolated and labeled with fluorophores as described (Greber et al., 1996; Greber et al., 1993; Nagel et al., 2003). EdU, F-ara-EdU, EdC, EdA and Tris(hydroxypropyltriazolyl)methylamine (THPTA) (Hong et al., 2009) were synthesized as described (Guan et al., 2011; Neef and Luedtke, 2011; Neef et al., 2012; Salic and

Mitchison, 2008). EdA/EdC-HAdV-C5 was propagated in A549 cells in presence of 2.5 μM EdA and EdC, added 11 h pi for 3 days, and purified by double CsCl equilibrium gradient centrifugations. Tissue culture infectious dose 50 ($TCID_{50}$) assays were performed with A549 cells infected with HAdV-C5 (MOI = 2) in presence of ethynyl-nucleosides, supernatants harvested 3 days pi and added to A549 cells in 96-well plates. Cells were fixed after 3 days, and plates stained with crystal violet. Relative infectious units were calculated as described (Puntener et al., 2011).

Mature virions of wild-type (WT) VACV strain Western Reserve (WR) were produced in BSC-40 cells and purified from cytoplasmic lysates (Mercer and Helenius, 2008). For EdU incorporation into viral genomes, we used VACV WR mCherry-A4 encoding a fluorescent version of the bona-fide core protein A4 in the endogenous locus (Schmidt et al., 2011). Inoculum was incubated with BSC-40 cells in DMEM without supplements at 37°C for 30 min (MOI 1), and progeny virus produced in full medium containing 1 μM EdU up to 48 h. For virus yield determination, BSC-40 cells were washed, suspended in 1mM Tris-HCl pH 9.0 and disrupted by three consecutive freeze/thaw cycles. Lysates were added to fresh BSC-40 cells and plaques counted 48 h pi.

Copper(I)-catalyzed azide alkyne cycloaddition (click) staining and immune-fluorescence microscopy

Samples were fixed in 4% paraformaldehyde for 15 min, quenched with 25 mM ammonium chloride, permeabilised with 0.5% Triton X-100 at room temperature for 5 min and labeled with primary and fluorophore-conjugated secondary antibodies. Samples were stained with freshly prepared click staining mix containing 10 μM Alexa-Fluor-594 or 488-azide, 1 mM CuSO4 and 10 mM sodium ascorbate in PBS in presence of 1 mM THPTA, and 10 mM amino-guanidine (AG) for protection against oxidative damage, at RT for 2 h in the dark, or 30 min in case of VACV (Hong et al., 2010). Samples were stained with 4',6-diamidino-2-phenylindole (DAPI, Molecular Probes, Leiden, The Netherlands) or DRAQ5 (Biostatus, Leicestershire, UK) for total DNA, embedded in DAKO medium (Dako Schweiz AG, Baar, Switzerland) for imaging by confocal

microscopy, or ProLong® Gold antifade reagent (Life Technologies, Carlsbad, U.S.A.) for gSTED microscopy. Fluorescence images were recorded on Leica SP5 confocal laser scanning microscope or Zeiss LSM510 Meta confocal system. EdU labeled VACV infected cells and viruses were stained with the detection Click-iT® EdU-Alexa-Fluor® 488 Imaging Kit (Invitrogen, Life Technologies, Baar, Switzerland). Viruses were seeded on a coverslip, fixed with 3.5% PFA, permeablised with 0.5% Triton-X and stained with Alexa-Fluor-488-azide.

gSTED

Super-resolution images were acquired with Leica SP8 gated STED microscope, with a pixel size of 19.99 nm. Image analysis was done on the raw data with custom programmed scripts using MATLAB software (MathWorks,Inc. Natick, MA, USA). To quantify and compare the size of punctate signals in regular confocal and gSTED images, we fitted the line profiles across the center of puncta with Gaussian curves by adaptive least-squares curve-fitting and calculated the full width at half maximum (FWHM). For area estimations, we fitted two dimensional Gaussian surfaces to our images. To reduce the noise and improve the quality of the fitting, images were pre-processed with edge preserving averaging filter. The fitting was done using non-linear least squares regression. Two FWHM of the fitted surface were calculated along the major and minor axes of the elliptic signal, and used to calculate the area of the signal. The goodness of the fits was evaluated using freedom adjusted R-square statistics. We took into account only the images where the fitting had R-square values above 0.5, and presented the results as frequency distribution plots.

Subcellular localization analyses

Images were recorded with Leica SP5 confocal microscope equipped with 63x (oil immersion, numerical aperture 1.4) objective. Image stacks had 0.5 µm steps and 2x averaging. vDNA, capsid, protein VII puncta were analysed by maximum projections of image stacks and processed by a local adaptive threshold method to generate an image masks for each particle. This image mask was used to measure average fluorescent

intensities over the particle areas. Cell shape was identified from over-exposed vDNA signals. The perimeters of cell nuclei in DAPI images were determined by global thresholding. The nuclear region was defined as the thresholded DAPI signal including 0.4 µm of the adjacent cytoplasm. The cytoplasmic area was between the nuclear region and the cell edge.

For quantification of vDNA and protein VII in the nucleus, we considered only sections through the center of the nucleus, where the DAPI area was in best focus and the hexon outside the DAPI signal. vDNA or protein VII puncta within the DAPI and the hexon areas were scored as imported material. Puncta that were more intense in the next upper or lower optical sections were counted as nuclear in these other sections. Puncta that were most intense in sections beyond the center of the nucleus were not considered as imported, thereby underestimating the levels of import. Nuclear import of vDNA positive for protein VII was also estimated in maximal projections of image stacks over the DAPI region. Results were presented on a per cell basis in scatter plots and fitted using linear-regression by GraphPad Prism software (GraphPad Software, Inc. La Jolla, CA, USA).

Streptolysin O

SLO was kindly provided by M. Husmann and S. Bhakdi (University Medical Center, Johannes Gutenberg-University Mainz). EdA/EdC-HAdV-C5 (1 µg) was bound to HeLa-ATCC cells (grown in 24 wells on glass coverslips) on ice for 60 min, and virus internalized at 37°C. SLO was bound to the plasma membrane and cells permeabilised by brief incubation at 37°C, click-stained with perfused Alexa-Fluor-594-azide at room temperature for 60 min, fixed, permeabilised with TX-100 and immune-stained against hexon (Suomalainen et al., 2013). Identical procedure was used for HAdV-C2_TS1 labeled with Alexa-488, except that cytosolic virus was detected with anti-Alexa-Fluor-488 antibodies.

Cells culture, antibodies, chemicals and *In situ* hybridization

See Supplemental Information

References

Belmont, A.S., and Straight, A.F. (1998). In vivo visualization of chromosomes using lac operator-repressor binding. Trends Cell Biol *8*, 121-124.

Besse, S., and Puvion-Dutilleul, F. (1994). High resolution localization of replicating viral genome in adenovirus-infected hela cells. Eur J Cell Biol *63*, 269-279.

Bremner, K.H., Scherer, J., Yi, J., Vershinin, M., Gross, S.P., and Vallee, R.B. (2009). Adenovirus transport via direct interaction of cytoplasmic dynein with the viral capsid hexon subunit. Cell Host Microbe *6*, 523-535.

Burckhardt, C.J., and Greber, U.F. (2009). Virus movements on the plasma membrane support infection and transmission between cells. PLoS Pathog *5*, e1000621.

Burckhardt, C.J., Suomalainen, M., Schoenenberger, P., Boucke, K., Hemmi, S., and Greber, U.F. (2011). Drifting motions of the adenovirus receptor CAR and immobile integrins initiate virus uncoating and membrane lytic protein exposure. Cell Host Microbe *10*, 105-117.

Chen, J., Morral, N., and Engel, D.A. (2007). Transcription releases protein VII from adenovirus chromatin. Virology *369*, 411-422.

Engelke, M.F., Burckhardt, C.J., Morf, M.K., and Greber, U.F. (2011). The dynactin complex enhances the speed of microtubule-dependent motions of adenovirus both towards and away from the nucleus. Viruses *3*, 233-253.

Gastaldelli, M., Imelli, N., Boucke, K., Amstutz, B., Meier, O., and Greber, U.F. (2008). Infectious adenovirus type 2 transport through early but not late endosomes. Traffic *9*, 2265-2278.

Gierlich, J., Burley, G.A., Gramlich, P.M., Hammond, D.M., and Carell, T. (2006). Click chemistry as a reliable method for the high-density postsynthetic functionalization of alkyne-modified DNA. Org Lett *8*, 3639-3642.

Greber, U.F., Suomalainen, M., Stidwill, R.P., Boucke, K., Ebersold, M., and Helenius, A. (1997). The role of the nuclear pore complex in adenovirus DNA entry. EMBO J *16*, 5998-6007.

Greber, U.F., Webster, P., Weber, J., and Helenius, A. (1996). The role of the adenovirus protease on virus entry into cells. EMBO J *15*, 1766-1777.

Greber, U.F., Willetts, M., Webster, P., and Helenius, A. (1993). Stepwise dismantling of adenovirus 2 during entry into cells. Cell *75*, 477-486.

Guan, L., van der Heijden, G.W., Bortvin, A., and Greenberg, M.M. (2011). Intracellular detection of cytosine incorporation in genomic DNA by using 5-ethynyl-2'-deoxycytidine. Chembiochem *12*, 2184-2190.

Hell, S.W., and Wichmann, J. (1994). Breaking the diffraction resolution limit by stimulated emission: stimulated-emission-depletion fluorescence microscopy. Opt Lett *19*, 780-782.

Hong, V., Presolski, S.I., Ma, C., and Finn, M.G. (2009). Analysis and optimization of copper-catalyzed azide-alkyne cycloaddition for bioconjugation. Angew Chem Int Ed Engl *48*, 9879-9883.

Hong, V., Steinmetz, N.F., Manchester, M., and Finn, M.G. (2010). Labeling live cells by copper-catalyzed alkyne--azide click chemistry. Bioconjugate chemistry *21*, 1912-1916.

Johnson, J.S., Osheim, Y.N., Xue, Y., Emanuel, M.R., Lewis, P.W., Bankovich, A., Beyer, A.L., and Engel, D.A. (2004). Adenovirus protein VII condenses DNA, represses transcription, and associates with transcriptional activator E1A. J Virol *78*, 6459-6468.

Kilcher, S., Schmidt, F.I., Schneider, C., Kopf, M., Helenius, A., and Mercer, J., . (2013). siRNA screen of early poxvirus genes identifies viral AAA+ ATPase as the genome-uncoating factor. submitted.

Kolb, H.C., Finn, M.G., and Sharpless, K.B. (2001). Click chemistry: diverse chemical function from a few good reactions. Angew Chem Int Ed Engl *40*, 2004-2021.

Komatsu, T., Haruki, H., and Nagata, K. (2011). Cellular and viral chromatin proteins are positive factors in the regulation of adenovirus gene expression. Nucleic Acids Res *39*, 889-901.

Leung, C.H., Chan, D.S., He, H.Z., Cheng, Z., Yang, H., and Ma, D.L. (2012). Luminescent detection of DNA-binding proteins. Nucleic Acids Res *40*, 941-955.

Lipovsky, A., Popa, A., Pimienta, G., Wyler, M., Bhan, A., Kuruvilla, L., Guie, M.A., Poffenberger, A.C., Nelson, C.D., Atwood, W.J.*, et al.* (2013). Genome-wide siRNA screen identifies the retromer as a cellular entry factor for human papillomavirus. Proc Natl Acad Sci U S A *110*, 7452-7457.

Lu, J., Li, F., Murphy, C.S., Davidson, M.W., and Gilbert, D.M. (2010). G2 phase chromatin lacks determinants of replication timing. J Cell Biol *189*, 967-980.

Marazzi, I., Ho, J.S., Kim, J., Manicassamy, B., Dewell, S., Albrecht, R.A., Seibert, C.W., Schaefer, U., Jeffrey, K.L., Prinjha, R.K.*, et al.* (2012). Suppression of the antiviral response by an influenza histone mimic. Nature *483*, 428-433.

Mercer, J., and Greber, U.F. (2013). Virus interactions with endocytic pathways in macrophages and dendritic cells. Trends Microbiol *21*, 380-388.

Mercer, J., and Helenius, A. (2008). Vaccinia virus uses macropinocytosis and apoptotic mimicry to enter host cells. Science *320*, 531-535.

Nagel, H., Maag, S., Tassis, A., Nestle, F.O., Greber, U.F., and Hemmi, S. (2003). The alphavbeta5 integrin of hematopoietic and nonhematopoietic cells is a transduction receptor of RGD-4C fiber-modified adenoviruses. Gene Ther *10*, 1643-1653.

Nakano, M.Y., Boucke, K., Suomalainen, M., Stidwill, R.P., and Greber, U.F. (2000). The first step of adenovirus type 2 disassembly occurs at the cell surface, independently of endocytosis and escape to the cytosol. J Virol *74*, 7085-7095.

Nakano, M.Y., and Greber, U.F. (2000). Quantitative microscopy of fluorescent adenovirus entry. J Struct Biol *129*, 57-68.

Nass, K., and Frenkel, G.D. (1980). Adenovirus-specific DNA-binding protein inhibits the hydrolysis of DNA by DNase in vitro. J Virol *35*, 314-319.

Neef, A.B., and Luedtke, N.W. (2011). Dynamic metabolic labeling of DNA in vivo with arabinosyl nucleosides. Proc Natl Acad Sci USA *108*, 20404-20409.

Neef, A.B., Samain, F., and Luedtke, N.W. (2012). Metabolic labeling of DNA by purine analogues in vivo. Chembiochem *13*, 1750-1753.

Nguyen, E.K., Nemerow, G.R., and Smith, J.G. (2010). Direct evidence from single-cell analysis that human {alpha}-defensins block adenovirus uncoating to neutralize infection. J Virol *84*, 4041-4049.

Puntener, D., Engelke, M.F., Ruzsics, Z., Strunze, S., Wilhelm, C., and Greber, U.F. (2011). Stepwise loss of fluorescent core protein V from human adenovirus during entry into cells. J Virol *85*, 481-496.

Puntener, D., and Greber, U.F. (2009). DNA-tumor virus entry - from plasma membrane to the nucleus. Sem Cell Dev Biol *20*, 631-642.

Qu, D., Wang, G., Wang, Z., Zhou, L., Chi, W., Cong, S., Ren, X., Liang, P., and Zhang, B. (2011). 5-Ethynyl-2'-deoxycytidine as a new agent for DNA labeling: detection of proliferating cells. Anal Biochem *417*, 112-121.

Reddy, V.S., Natchiar, S.K., Stewart, P.L., and Nemerow, G.R. (2010). Crystal structure of human adenovirus at 3.5 A resolution. Science *329*, 1071-1075.

Ross, P.J., Kennedy, M.A., Christou, C., Risco Quiroz, M., Poulin, K.L., and Parks, R.J. (2011). Assembly of helper-dependent adenovirus DNA into chromatin promotes efficient gene expression. J Virol *85*, 3950-3958.

Salic, A., and Mitchison, T. (2008). A chemical method for fast and sensitive detection of DNA synthesis in vivo. Proc Natl Acad Sci USA *105*, 2415-2420.

Schmidt, F.I., Bleck, C.K., Helenius, A., and Mercer, J. (2011). Vaccinia extracellular virions enter cells by macropinocytosis and acid-activated membrane rupture. EMBO J *30*, 3647-3661.

Stiefel, P., Schmidt, F.I., Dorig, P., Behr, P., Zambelli, T., Vorholt, J.A., and Mercer, J. (2012). Cooperative vaccinia infection demonstrated at the single-cell level using FluidFM. Nano Lett *12*, 4219-4227.

Strunze, S., Engelke, M.F., Wang, I.-H., Puntener, D., Boucke, K., Schleich, S., Way, M., Schoenenberger, P., Burckhardt, C.J., and Greber, U.F. (2011). Kinesin-1-mediated capsid disassembly and disruption of the nuclear pore complex promote virus infection. Cell Host Microbe *10*, 210-223.

Strunze, S., Trotman, L.C., Boucke, K., and Greber, U.F. (2005). Nuclear targeting of adenovirus type 2 requires CRM1-mediated nuclear export. Mol Biol Cell *16*, 2999-3009.

Suomalainen, M., Luisoni, S., Engel, D.A., Bianchi, S., Boucke, K., and Greber, U.F. (2013). A direct and versatile assay measuring membrane penetration of adenovirus in single cells. J Virol *in press*.

Tan, W., Wang, K., and Drake, T.J. (2004). Molecular beacons. Curr Opin Chem Biol *8*, 547-553.

Tate, V.E., and Philipson, L. (1979). Parental adenovirus DNA accumulates in nucleosome-like structures in infected cells. Nucleic Acids Res *6*, 2769-2785.

Trotman, L.C., Mosberger, N., Fornerod, M., Stidwill, R.P., and Greber, U.F. (2001). Import of adenovirus DNA involves the nuclear pore complex receptor CAN/Nup214 and histone H1. Nature Cell Biology *3*, 1092-1100.

van der Vliet, P.C., Keegstra, W., and Jansz, H.S. (1978). Complex formation between the adenovirus type 5 DNA-binding protein and single-stranded DNA. Eur J Biochem *86*, 389-398.

Vayda, M.E., Rogers, A.E., and Flint, S.J. (1983). The structure of nucleoprotein cores released from adenovirions. Nucleic Acids Res *11*, 441-460.

Voelkerding, K., and Klessig, D.F. (1986). Identification of two nuclear subclasses of the adenovirus type 5-encoded DNA-binding protein. J Virol *60*, 353-362.

Walev, I., Bhakdi, S.C., Hofmann, F., Djonder, N., Valeva, A., Aktories, K., and Bhakdi, S. (2001). Delivery of proteins into living cells by reversible membrane permeabilization with streptolysin-O. Proc Natl Acad Sci USA *98*, 3185-3190.

Walkiewicz, M.P., Morral, N., and Engel, D.A. (2009). Accurate single-day titration of adenovirus vectors based on equivalence of protein VII nuclear dots and infectious particles. J Virol Methods *159*, 251-258.

Wang, M., Yuan, Y., and Liang, G. (2012). Click chemistry for molecular imaging. Current Molecular Imaging *1*, 87–95.

Willig, K.I., Harke, B., Medda, R., and Hell, S.W. (2007). STED microscopy with continuous wave beams. Nat Methods *4*, 915-918.

Wolfrum, N., and Greber, U.F. (2013). Adenovirus signalling in entry. Cell Microbiol *15*, 53-62.

Xue, Y., Johnson, J.S., Ornelles, D.A., Lieberman, J., and Engel, D.A. (2005). Adenovirus protein VII functions throughout early phase and interacts with cellular proteins SET and pp32. J Virol *79*, 2474-2483.

Yakimovich, A., Gumpert, H., Burckhardt, C.J., Lutschg, V.A., Jurgeit, A., Sbalzarini, I.F., and Greber, U.F. (2012). Cell-free transmission of human adenovirus by passive mass transfer in cell culture simulated in a computer model. J Virol *86*, 10123–10137.

Acknowledgements

We thank U. Ziegler and J. Doehner (Center for Microscopy, University of Zurich) for their expert help with STED microscopy, and A. Yakimovich and A. Jurgeit for discussions. This work was financed by the Swiss National Science Foundation (grants 31003A_141222/1 and 316030_145037 to UFG, and grant 146754 to NWL), an Initial Training Networks grant from the European Union (AdVance) to UFG, the University of

Zürich Forschungskredit (57131902 to AN), and a scholarship from the Taiwanese government (Ministry of Education) to IW.

Contributions

UFG conceived and directed the study. UFG, IW, MS, SK, JM, AN, NL designed experiments, AN, NL provided ethynyl-modified nucleosides, VA performed statistical analyses and Gaussian fittings, IW performed fluorescence microscopy experiments in confocal and gSTED modes with isolated HAdV, and HAdV or HSV-1 infected cells, and determined nuclear import of vDNA and protein VII in single sections or maximal projections. MS prepared ethynyl-modified HAdV, and carried out FISH assays and SLO permeabilisation experiments with HAdV-C5 and TS1. SK performed the VACV experiments under the supervision of JM. UFG, IW, MS, NWL, SK and JM wrote the manuscript.

Figure Legends

Fig. 1: Incorporation of ethynyl-modified nucleosides into adenovirus replication sites of human lung epithelial cells

(a, b) Infection of A549 cells with HAdV-C5 (MOI 30) in presence of ethynyl-modified nucleoside (2.5 µM) from 4 to 16 h (a) or 24 h pi (b), respectively. Shown are single sections across the center of the cells. Scale bar: 10 µm.

(c) Single step growth curves for HAdV-C5 (MOI 2, 72 h) in A549 cells in presence of different concentrations of ethynyl-modified nucleoside added 8 h pi. DMSO and mock infections (without DMSO) yielded 31786 and 30690 relative infectious units with standard deviations of 2584 and 2979 units from n=3 measurements, respectively. (d) Determination of viral titers by infectious dose 50 ($TCID_{50}$).

(e) Comparison of FISH and click chemistry procedures for detection of newly synthesized HAdV-C5 vDNA in the nucleus of A549 cells 16 h pi. Note the superior spatial resolution and signal to noise from EdC labeled cells. Scale bar: 5 µm.

Fig. 2: Incorporation of EdA/EdC into HAdV-C5

Single virus analyses of native and heat disrupted EdA/EdC-HAdV-C5 and unlabeled HAdV-C5 on poly-lysine-coated glass cover slips. Examples of triple positive structures (hexon, protein VII antibodies, alexa-488-azide) highlighted by open arrowheads. Filled arrowheads point to vDNA and protein VII positive puncta lacking hexon staining, possibly owing to weak labeling with 9C12, or loss during heat treatment. Arrow denotes a virus negative for vDNA and protein VII staining, similar to unbroken viruses. Scale bar: 2 µm.

Fig. 3: Incorporation of EdU into VACV replication sites and particles

(a) BSC-40 cells were pre-loaded with nucleoside analogue or DMSO for 24 h, and cells infected with VACV for 5 h in presence of nucleosides. Replication factories were

indicated by the viral mCherry-A4. Newly synthesized genome-labeled viruses were observed with EdU (boxed area, arrow head) and EdC (arrow head). Scale bar: 10 µm.

(b) Virus yield from BSC-40 cells in presence of nucleoside analogues 24 h pi. Shown are the mean values including the standard errors.

(c) Particle analyses of isolated EdU-VACV-WR mCherry-A4. Scale bar: 5 µm.

Related to Figure S1.

Fig. 4: Capsid-associated and free vDNA detected in cells at single molecule resolution

(a) Maximal projections of image stacks of incoming EdA/EdC-HAdV-C5 probed with Alexa-Fluor-594-azide, and 9C12 anti-hexon antibody. Scale bar: 10 µm.

(b) Mean values including standard deviations of capsid-associated vDNA and per cent of vDNA-positive capsids during entry in presence or absence of leptomycin B (LMB).

(c, d) Dual color confocal and parallel gSTED images of capsids stained with anti-hexon antibody and a secondary antibody conjugated to Abberior STAR 440SX dye. vDNA was stained with Alexa-Fluor-488-azide 30 min (c) or 90 min pi (d). Arrows denote empty capsids and arrowheads capsid-free vDNA. Scale bar: 0.5 µm.

(e) Estimation of the diameter of particle signals (Gaussian fit to the line profile of the dash-line indicated). Full width at half maximal peak (FWHM) determined with gSTED (red) and regular confocal microscopy (black).

(f) Area estimation of vDNA signals by Gaussian surface fitting and ellipse calculation using FWHM.

(g) Frequency analysis of estimated areas of capsid-associated and free.

Fig. 5: Capsid-associated and capsid-free vDNA are cytosolic

(a) Time course of HeLa cell infections with EdA/EdC-HAdV-C5 in presence or absence of LMB. Asterisks denote nuclear background structures. Scale bar: 10 µm.

(b) Schematic representation of procedure in (a).

(c) Endosomal membranes remain intact upon SLO permeabilisation. Note that TS1 internalized for 60 min remains undetected in SLO permeabilised cells and is only detected upon complete cell permeabilisation with TX-100. Scale bar: 10 µm.

(d) Schematic representation of procedure in (c).

Fig. 6: Delivery of incoming vDNA into the nucleus

(a) EdA/EdC-HAdV-C5 was bound to HeLa cells at cold (MOI 30), and samples were warmed for 150 min, fixed and processed for click chemistry detection of vDNA with Alexa-Fluor-594-azide (red) and immune-staining for hexon using 9C12 (green). Scale bar: 10 µm.

(b) Per cell based correlations of total vDNA, nuclear targeted vDNA, capsid-free vDNA and vDNA-less (empty) capsids with the number of viruses, including the standard errors of the mean (SEM).

(c) Plot of nuclear capsid-free vDNA puncta against viruses per cell with an R^2 value of 0.57 for 20-200 viruses per cell, but no apparent correlation above 200 particles per cell. Frequency analysis (left blue plot) with a fit based on log-normal distribution in red. Right blue plot shows the percentage of vDNA in the nucleus as a function of total viruses per cell, including a frequency analysis.

Related to Figure S2.

Fig. 7: Protein VII positive and negative pools of nuclear vDNA

(a) HeLa cells were infected with EdA/EdC-HAdV-C5 for 150 min, stained with Alexa-Fluor-594-azide and anti-protein VII antibodies and anti-rabbit IgG-Alexa-488, and analysed by confocal microscopy. Maximal projections of image stacks are shown. Arrows denote cytoplasmic vDNA devoid of protein VII. Scale bar: 10 µm.

(b) Per cell based correlation of vDNA positive for VII in the nucleus against viral dose (viruses) represented as numbers of puncta or per cent of total nuclear vDNA.

(c) Correlation of nuclear protein VII against viral dose.

(d) Correlation of vDNA-free protein VII against viral dose, represented as numbers of nuclear puncta or per cent of total nuclear protein VII.

F1

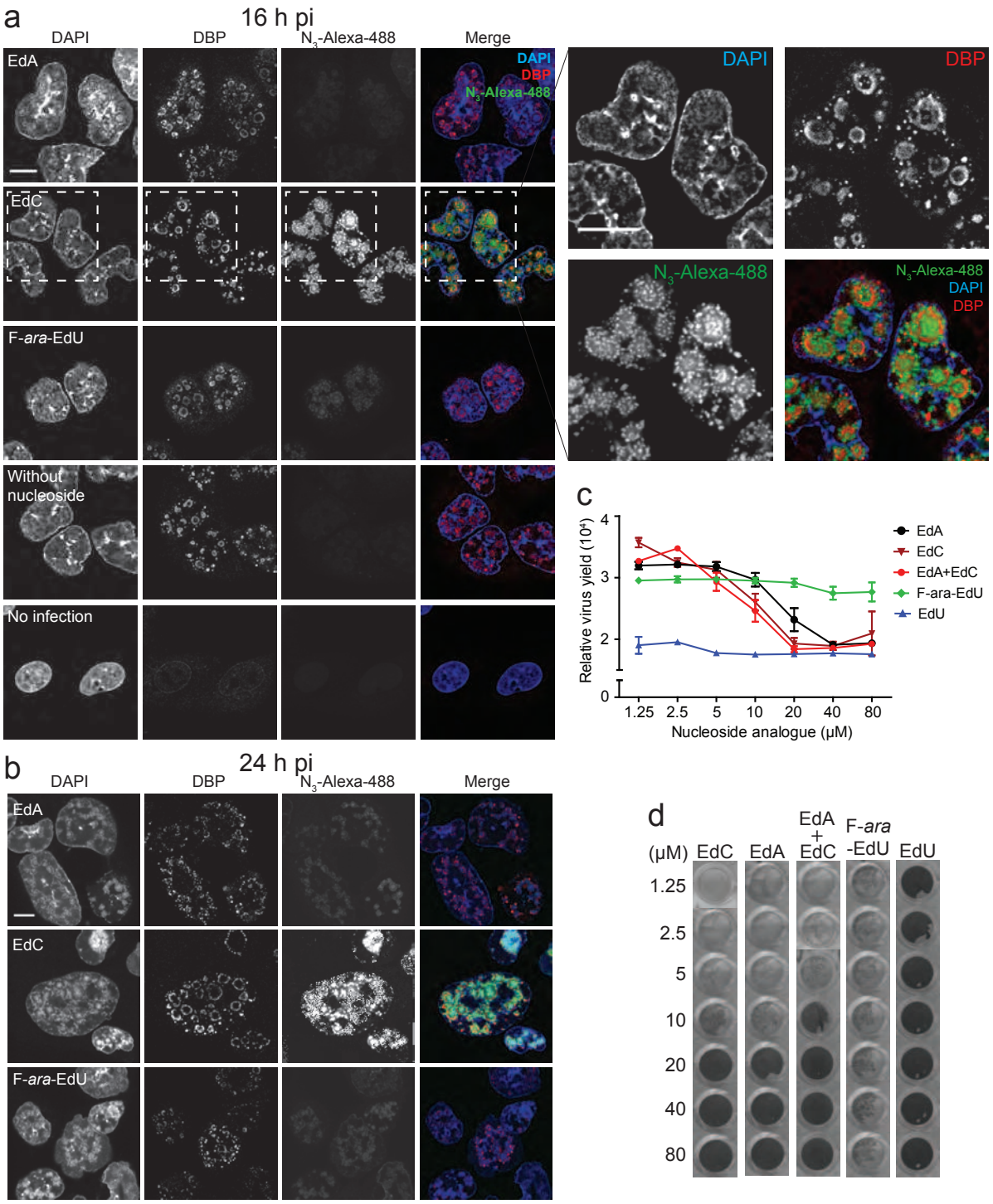
a
16 h pi
DAPI
DBP
N3-Alexa-488
Merge
EdA
EdC
F-ara-EdU
Without nucleoside
No infection
DAPI
DBP
N3-Alexa-488
DAPI
DBP
c
Relative virus yield (10⁴)
Nucleoside analogue (μM)
EdA
EdC
EdA+EdC
F-ara-EdU
EdU
b
24 h pi
d
(μM)
EdC
EdA
EdA + EdC
F-ara -EdU
EdU
e
FISH
EdC click chemistry
DAPI
vDNA

F2

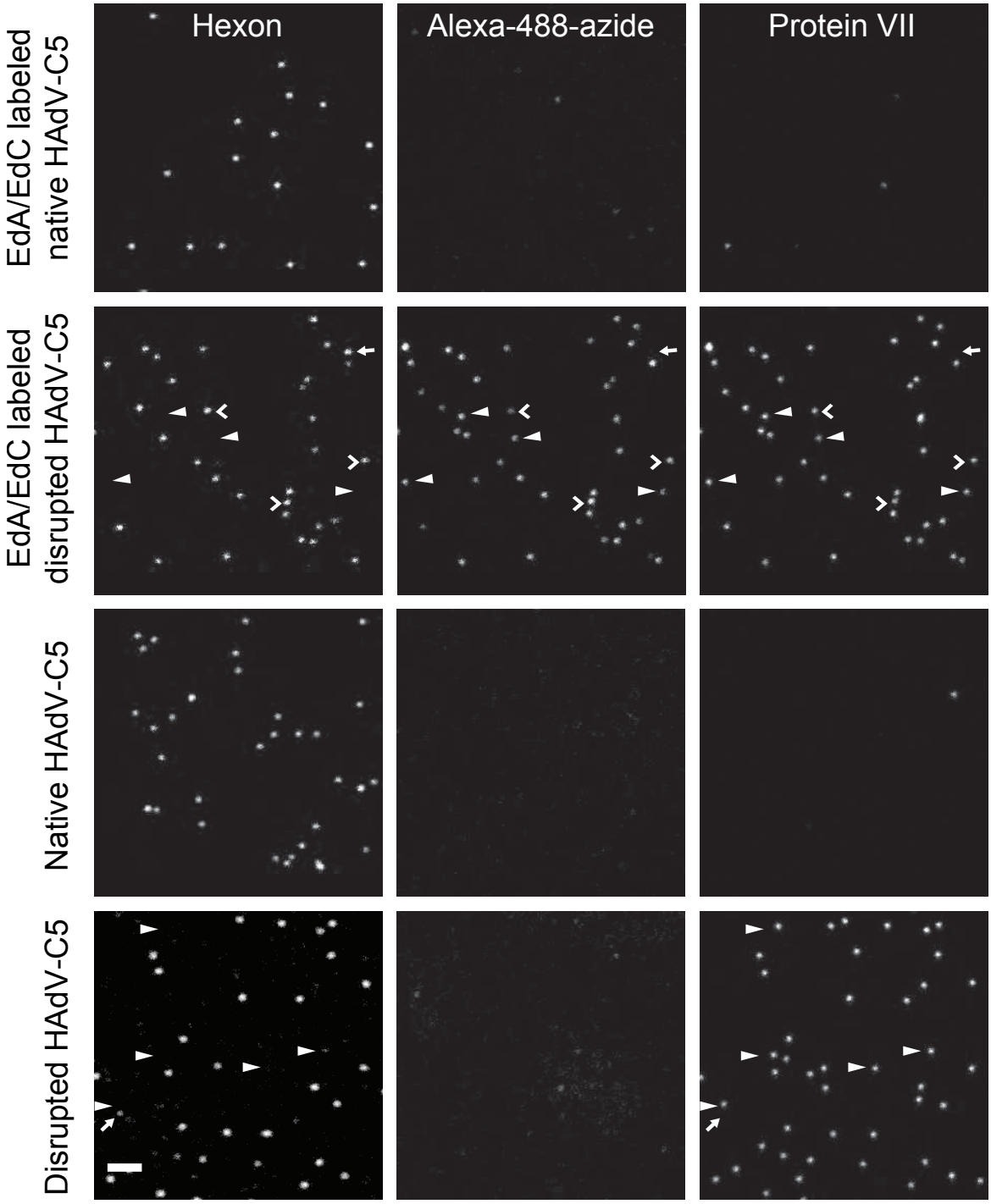
Hexon
Alexa-488-azide
Protein VII
EdA/EdC labeled native HAdV-C5
EdA/EdC labeled disrupted HAdV-C5
Native HAdV-C5
Disrupted HAdV-C5

F3

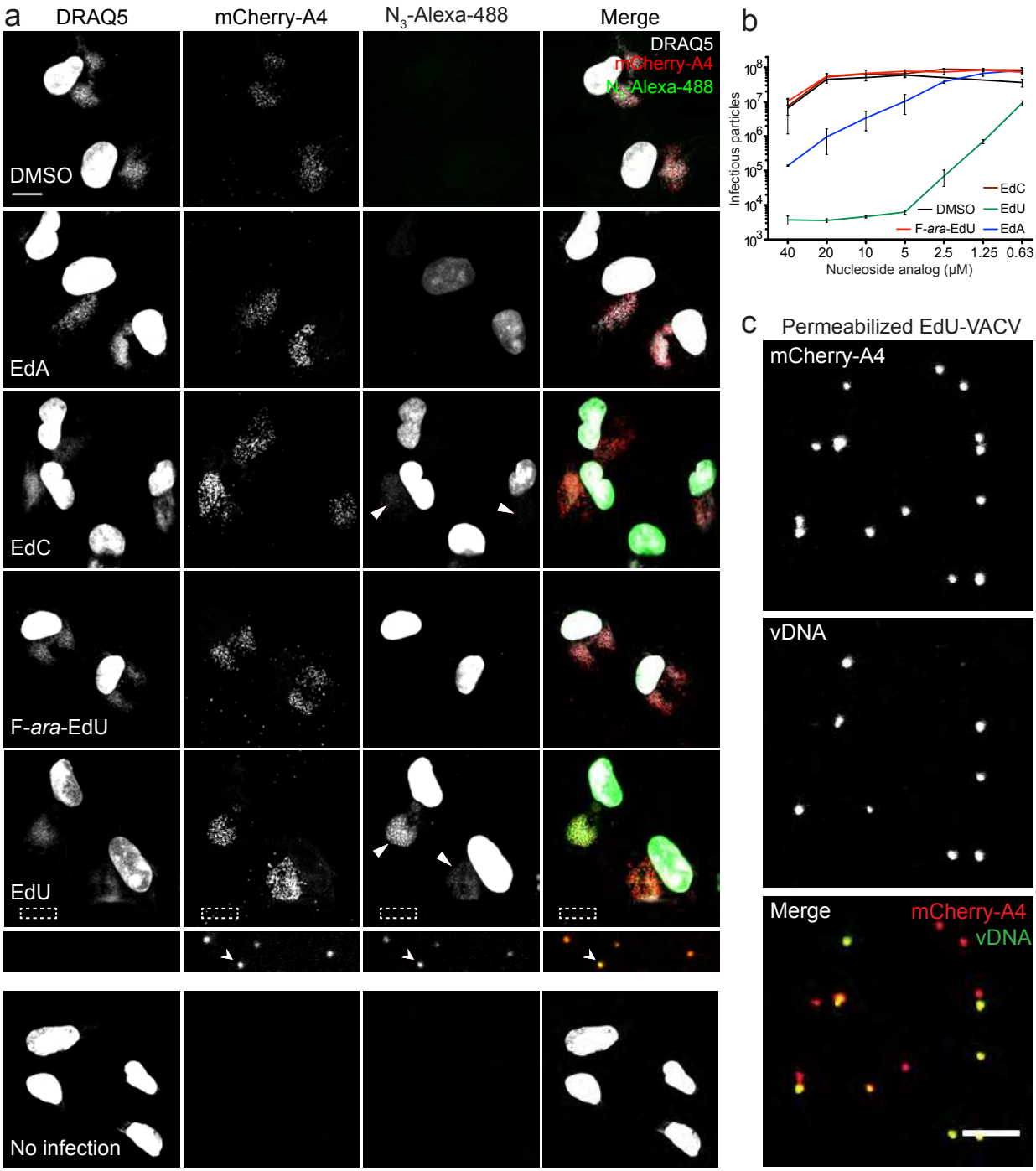
a
DRAQ5
mCherry-A4
N3-Alexa-488
Merge
DRAQ5
mCherry-A4
N3-Alexa-488
DMSO
EdA
EdC
F-ara-EdU
EdU
No infection
b
Infectious particles
Nucleoside analog (μM)
EdC
DMSO
EdU
F-ara-EdU
EdA
c
Permeabilized EdU-VACV
mCherry-A4
vDNA
Merge
mCherry-A4
vDNA

F4

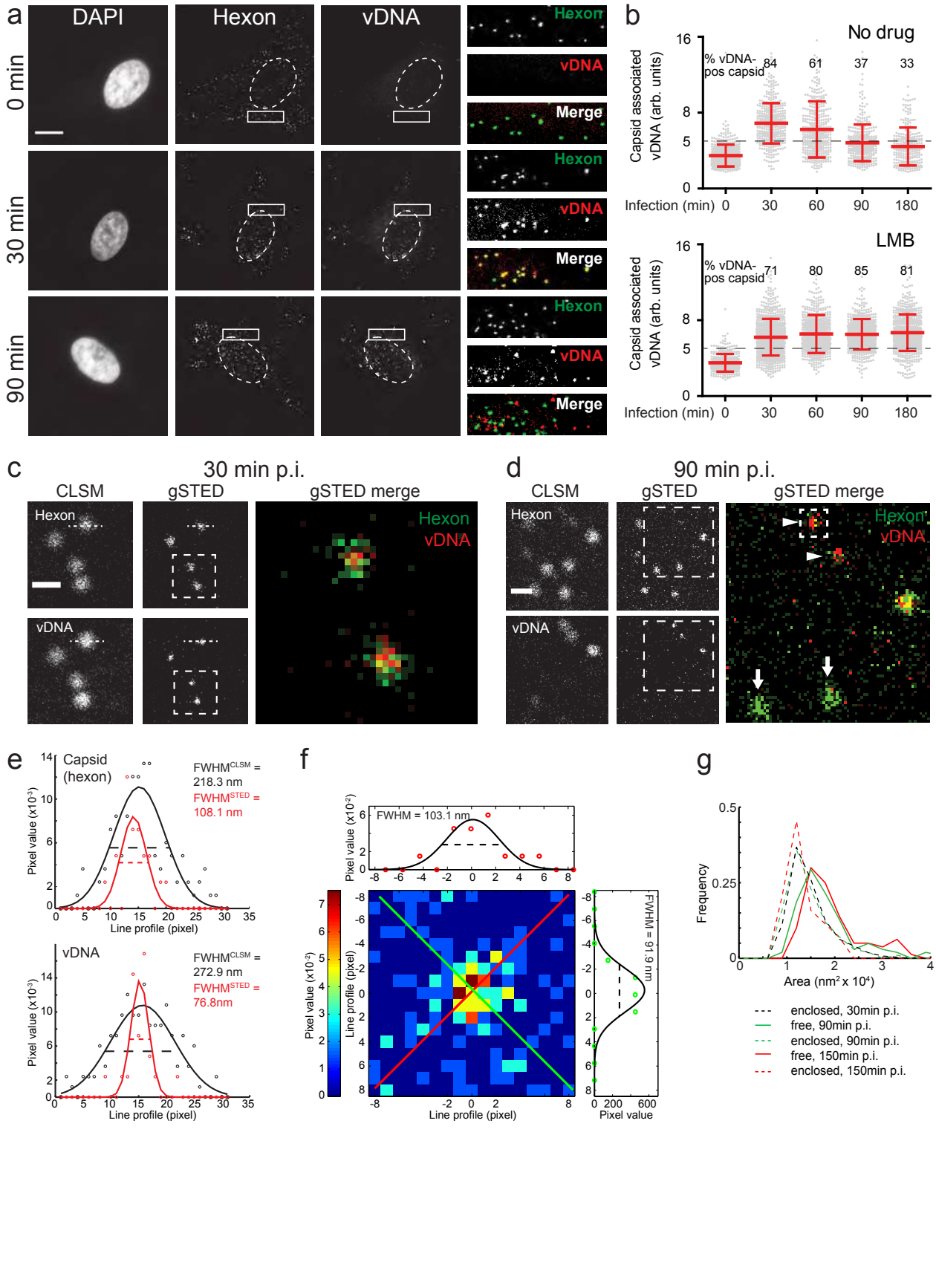
a
DAPI
Hexon
vDNA
0 min
30 min
90 min
Hexon
vDNA
Merge
b
No drug
% vDNA-pos capsid
84
61
37
33
Capsid associated vDNA (arb. units)
Infection (min) 0 30 60 90 180
LMB
71
80
85
81
c
30 min p.i.
CLSM
gSTED
gSTED merge
d
90 min p.i.
e
Capsid (hexon)
FWHM^CLSM = 218.3 nm
FWHM^STED = 108.1 nm
Pixel value (x10^-3)
Line profile (pixel)
vDNA
FWHM^CLSM = 272.9 nm
FWHM^STED = 76.8nm
f
FWHM = 103.1 nm
Pixel value (x10^-2)
Line profile (pixel)
FWHM = 91.9 nm
Pixel value
g
Frequency
Area (nm² x 10⁴)
enclosed, 30min p.i.
free, 90min p.i.
enclosed, 90min p.i.
free, 150min p.i.
enclosed, 150min p.i.

F5

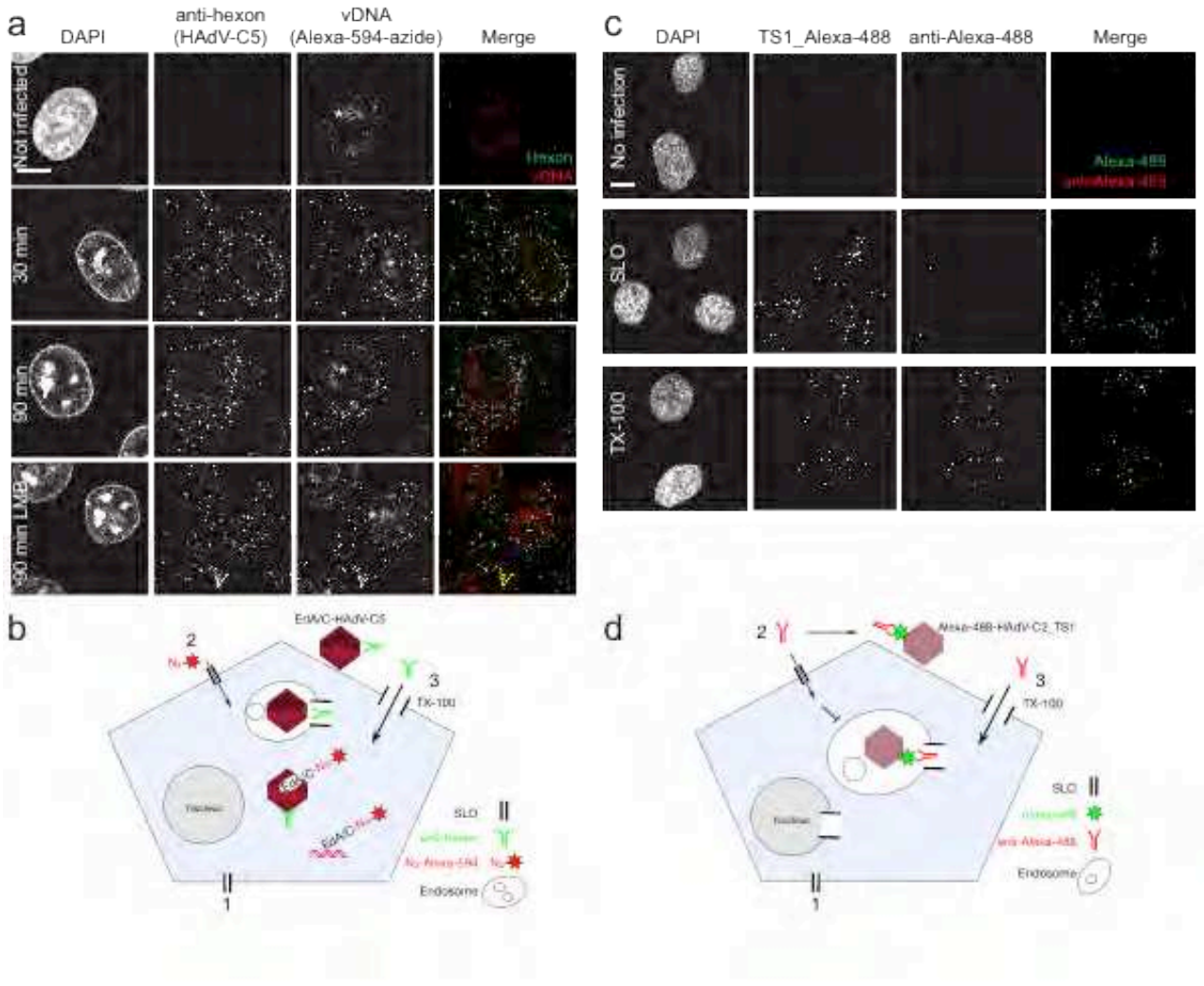
a
DAPI
anti-hexon (HAdV-C5)
vDNA (Alexa-594-azide)
Merge
Not infected
30 min
90 min
90 min LMB
c
DAPI
TS1_Alexa-488
anti-Alexa-488
Merge
No infection
SLO
TX-100
b
EdU
2
3
TX-100
SLO
Endosome
1
d
Alexa-488-HAdV-C2_TS1
2
3
TX-100
SLO
Endosome
1

F6

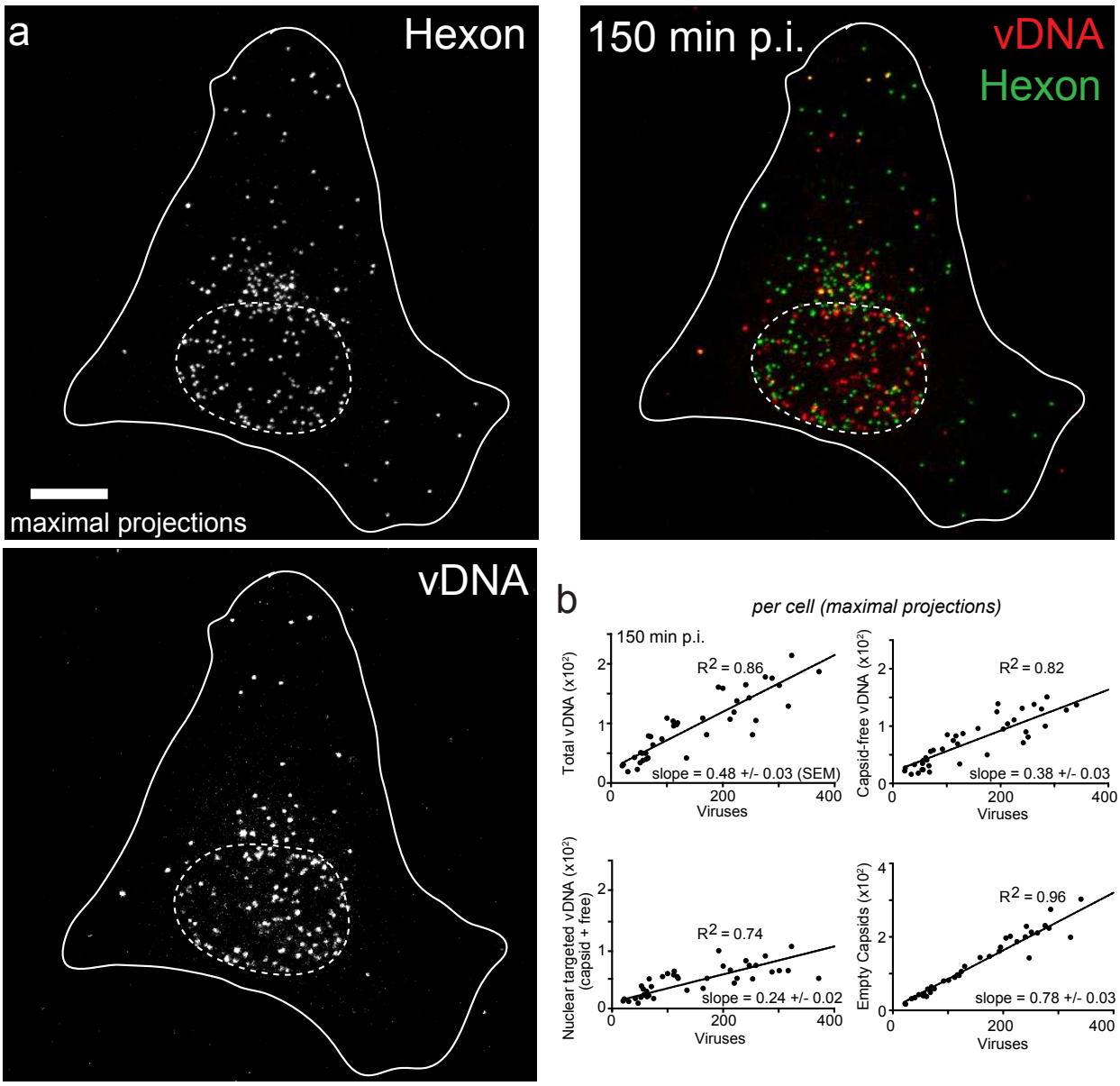
a
Hexon
maximal projections
150 min p.i.
vDNA
Hexon
vDNA
b
per cell (maximal projections)
150 min p.i.
R2 = 0.86
slope = 0.48 +/- 0.03 (SEM)
Total vDNA (x10²)
Viruses
R2 = 0.82
slope = 0.38 +/- 0.03
Capsid-free vDNA (x10²)
R2 = 0.74
slope = 0.24 +/- 0.02
Nuclear targeted vDNA (x10²) (capsid + free)
R2 = 0.96
slope = 0.78 +/- 0.03
Empty Capsids (x10²)
c
per cell (middle sections)
R2 = 0.57
Nuclear vDNA puncta (capsid-free)
per cell (middle sections)
Nuclear vDNA (% viruses)
Events
Nuclear vDNA (puncta)
Nuclear vDNA (% of viruses)

F7

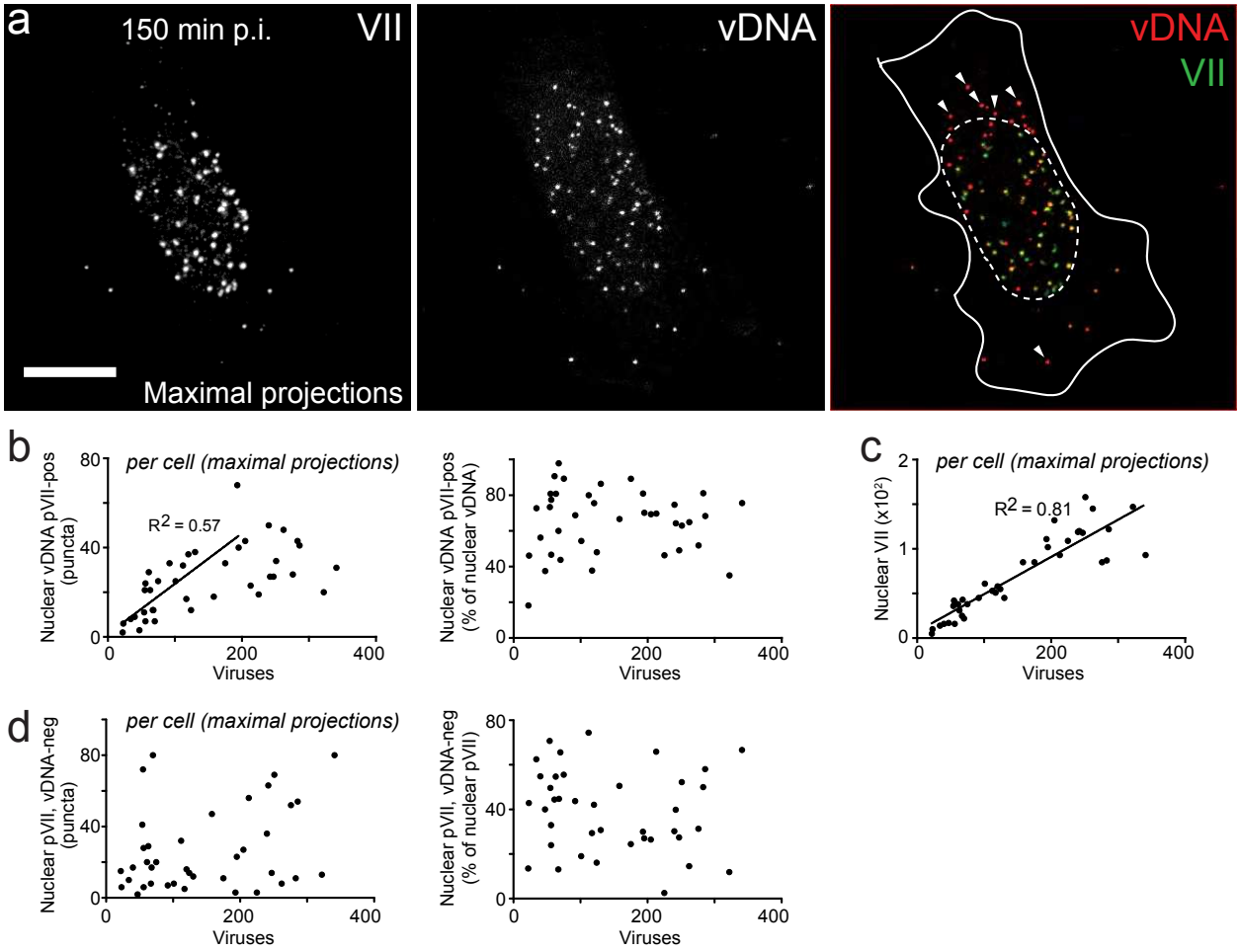
a
150 min p.i.
VII
Maximal projections
vDNA
vDNA
VII
b
per cell (maximal projections)
Nuclear vDNA pVII-pos (puncta)
R2 = 0.57
Viruses
Nuclear vDNA pVII-pos (% of nuclear vDNA)
Viruses
c
per cell (maximal projections)
Nuclear VII (x10²)
R2 = 0.81
Viruses
d
per cell (maximal projections)
Nuclear pVII, vDNA-neg (puncta)
Viruses
Nuclear pVII, vDNA-neg (% of nuclear pVII)
Viruses

Supplemental Information

Tracking viral genomes in host cells at single molecule resolution by click chemistry and super-resolution microscopy

I-Hsuan Wang, Maarit Suomalainen, Vardan Andriasyan, Samuel Kilcher, Jason Mercer, Anne Neef, Nathan W. Luedtke & Urs F. Greber

Supplemental Data

Figure S1: Metabolic labeling of herpes virus replication centers

HSV-1 replication centers were visualized in infected A549 cells 8 h pi. Each nucleoside (2.5 μM) was present in the medium starting from 1 h pi. Ethynyl-modified vDNA was stained using Alexa-Fluor-594-azide, and samples co-stained with DAPI and anti-ICP8 antibodies. Scale bar: 10 μm.

Related to Figure 3.

Figure S1

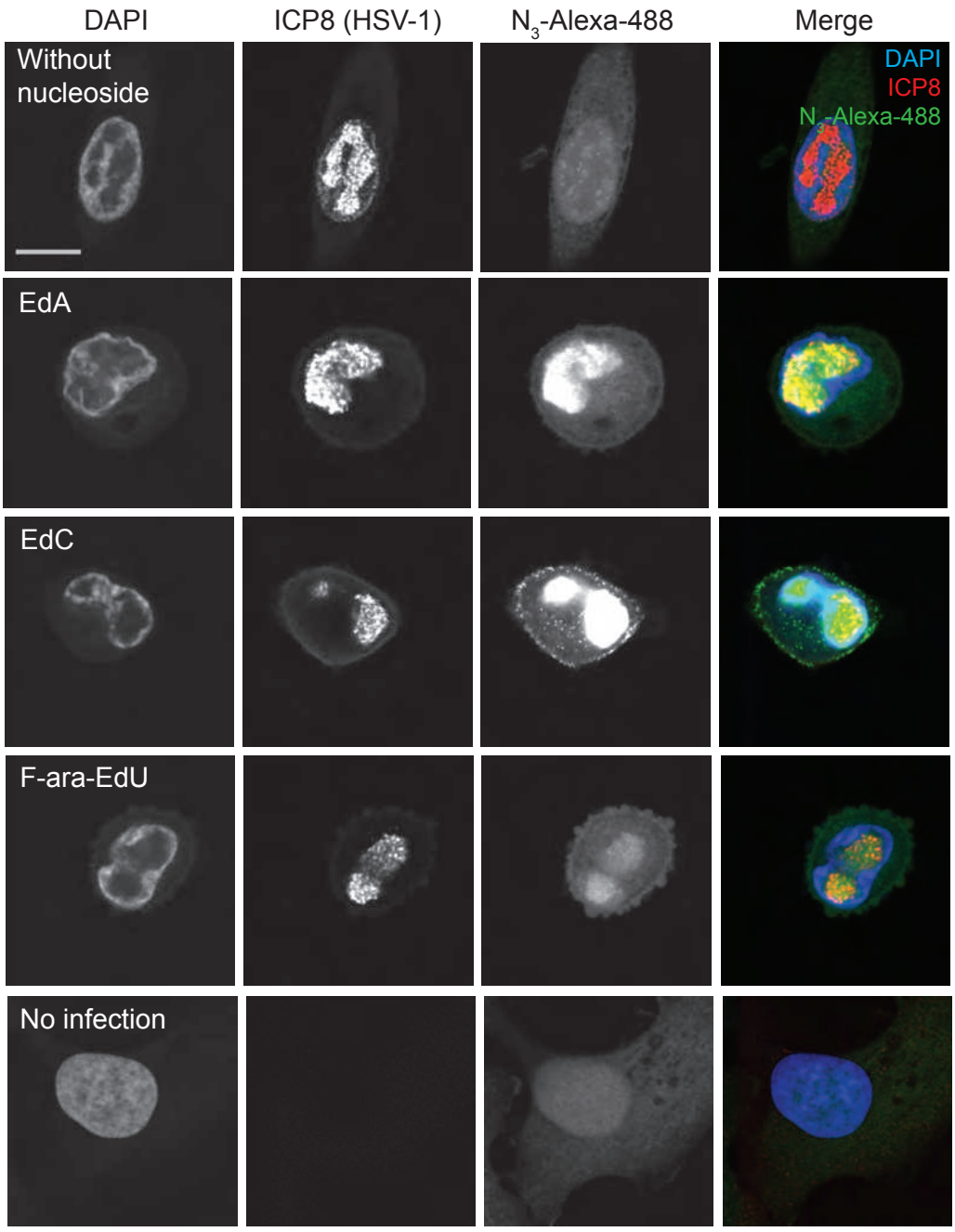
DAPI
ICP8 (HSV-1)
N3-Alexa-488
Merge
Without nucleoside
DAPI
ICP8
N3-Alexa-488
EdA
EdC
F-ara-EdU
No infection

Figure S2: Delivery of capsid-free vDNA from EdA/EdC-labeled HAdV-C5 into the nucleus and cytoplasm

(a) HeLa cells were infected with EdA/EdC-HAdV-C5 for 30 or 150 min, fixed and processed for *fluorescence in situ* hybridization (FISH). Single confocal microscopy sections across a central plane of the cells are shown. Scale bar: 10 µm.

(b) HeLa cells were infected with EdA/EdC-HAdV-C5 for 150 min (as described in panel c), processed for click chemistry labeling, stained with DAPI and Mab414 detecting nuclear pore complex antigens (Davis and Blobel, 1987), and analysed by confocal microscopy. Single mid plane sections across the nucleus were acquired with DAPI staining at 405 nm (blue), mouse monoclonal antibody (Mab) 414 and secondary Alexa-488 conjugated anti-mouse IgG at 488 nm (white pseudo-colored), vDNA with Alexa-Fluor-594-azide at 561 nm (red) and rabbit anti-protein VII and Alexa-633 conjugated anti-rabbit IgG at 633 nm excitation (green pseudo-colored). For details, see Fig. 6. Scale bar: 10 µm.

(c-d) Maximal projections of confocal images, including the staining for protein VII of the same cells as in Fig. 6. EdA/EdC-HAdV-C5 was bound to HeLa cells at cold (MOI 30 or 75), and samples were warmed for 150 min, fixed and processed for click chemistry detection of vDNA with Alexa-Fluor-594-azide (red), immune-staining for hexon using 9C12 (green) and protein VII (blue), imaged by confocal fluorescence microscopy and data represented as maximal projections of all the sections (b). A merged image is shown in (c). Scale bars = 10 µm.

(e) Per cell based correlations of nuclear targeted and cytoplasmic capsid-free nuclear vDNA with number of viruses.

(f) Plot of nuclear vDNA puncta against viruses per cell with an R^2 value of 0.57 for 20-200 viruses per cell, but no apparent correlation above 200 particles per cell. A frequency analysis is shown below in blue with a fit based on log-normal distribution in red. Percentage of nuclear vDNA of total viruses per cell, including a frequency analysis is shown on the right side.

(g) Analyses of nuclear vDNA (capsid-free puncta plus protein VII-positive puncta) in single confocal mid-sections. EdA/EdC labeled vDNA was probed by click staining with Alexa-Fluor-594-azide (white) 150 min pi, and samples stained for hexon (green), nuclei (DAPI, blue) and protein VII (white). Image stacks were acquired across the entire nucleus. To distinguish nuclear from cytoplasmic vDNA, we analysed single sections across the center of the nucleus, in which hexon was outside the nucleus, in this case sections 6 and 7. Note that hexon is largely outside the nucleus. White circles depict vDNA/protein VII puncta in the nucleus. Dotted white circles denote vDNA/pVII puncta that were more intense in the other optical section (6 or 7), and were counted as nuclear in this other section. White arrowheads point to particles that were most intense in sections beyond the center of the nucleus, and hence were not considered in this analysis. Scale bar: 10 μm.

Related to Figure 6.

Figure S2

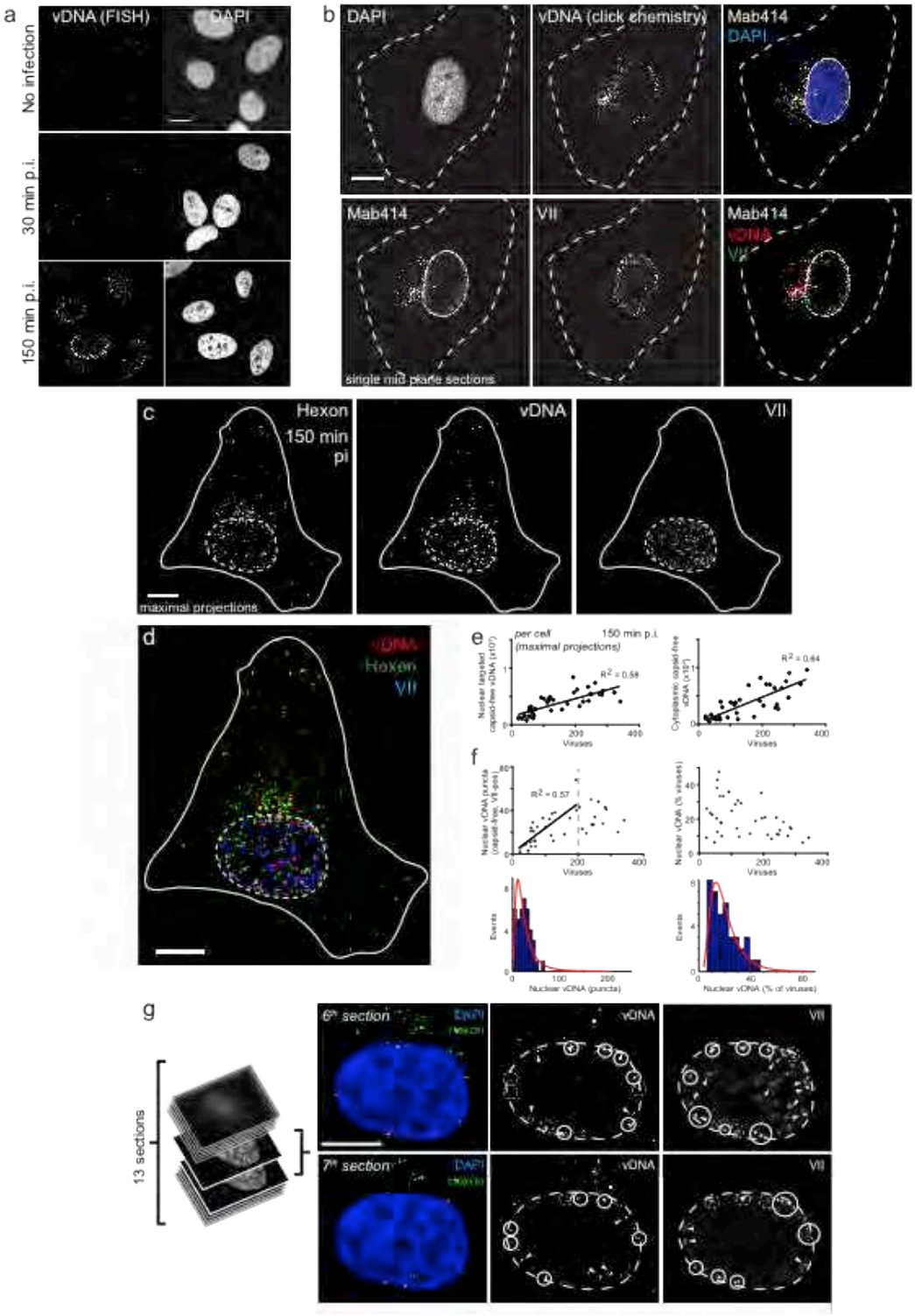
a
vDNA (FISH)
DAPI
No infection
30 min p.i.
150 min p.i.
b
DAPI
vDNA (click chemistry)
Mab414
DAPI
Mab414
VII
Mab414
vDNA
VII
single mid plane sections
c
Hexon
150 min
pi
vDNA
VII
maximal projections
d
vDNA
Hexon
VII
e
per cell
(maximal projections)
150 min p.i.
Viruses
f
Viruses
Events
Nuclear vDNA (puncta)
Nuclear vDNA (% of viruses)
g
13 sections
6th section
7th section
vDNA
VII

Supplemental Experimental Procedures

Cells culture, antibodies and chemicals

Human bronchial epithelial A549 cells and HeLa-ATCC (American Type Culture Collection) cells were grown at 37°C under 5% CO_2 in Dulbecco's modified Eagle's medium (DMEM) supplemented with 7.5 % FBS and 1% nonessential amino acids (Gibco-BRL). For BSC-40 (African green monkey kidney) cells DMEM was supplemented with 10% heat-inactivated FBS, glutamax, sodium pyruvate, non-essential amino acids, and penicillin-streptomycin.

Mouse monoclonal antibody 9C12 against HAdV-C5 hexon was developed by L. Fayadat-Dilman and W. Olijve and obtained from the Developmental Studies Hybridoma Bank developed under the auspices of the NICHD and maintained by The University of Iowa, Department of Biology,Iowa City, IA 52242 (Varghese et al., 2004). Guinea pig anti-DBP was provided by W. Deppert (Heinrich Pete Institute, Hamburg, Germany, Deppert et al., 1988). Rabbit anti-protein VII antibody was obtained from D. Engel (University of Virginia, U.S.A.) (Walkiewicz et al., 2009), and the monoclonal mouse antibody against HSV ICP8 was kindly provided by R. Heilbronn (Charité–University Medicine Berlin, Berlin, Germany). Mab414 developed by (Davis and Blobel, 1987) was purchased from Eurogentec, Seraing, Belgium. Rabbit anti-Alexa-Fluor-488, goat anti-mouse IgG coupled to Alexa-Fluor-488, 594 or 633 and Alexa-Fluor-488 or 594 conjugated to azide were purchased from Life Technologies (Carlsbad, U.S.A.). Goat anti-mouse IgG conjugated with Abberior STAR 440SX was from Abberior GmbH (Goettingen, Germany). LMB was from LC laboratories (Woburn, U.S.A.), and stored in ethanol at -20°C until use. AG was from Sigma-Aldrich (St. Louis, U.S.A.).

Labeling of Herpes simplex virus 1 (HSV-1) with clickable nucleosides

HSV-1-C12 is a recombinant HSV-1 strain SC16 containing an enhanced green fluorescent protein (eGFP) expression cassette in the US5 (gJ) locus, driven by human cytomegalovirus (HCMV) IE1 promoter. The virus was originally cloned by S. Efstathiou (University of Cambridge, Cambridge, United Kingdom), and working stocks kindly provided by C. Fraefel (University of Zurich, Zurich, Switzerland).

In situ hybridization

The in situ hybridization was done essentially as previously described (Greber et al., 1997), except that the Alexa-Fluor-594-labeled probe was prepared using FISH Tag^{TM} DNA Red Kit (Life Technologies), and the coverslips were inverted over 5 µl hybridization mix containing 10 ng of the labeled probe, 50% deionized formamide, 12.5 % dextran sulfate and 0.74×SSC. The 42°C and 60°C washing steps were omitted. For detection of the incoming virus genome, HeLa-ATCC cells grown on glass coverslips in 24-well dishes were incubated with EdA/EdC-HAdV-C5 (1 µg) at 37°C for 30 or 60 min, virus inoculum was removed and samples further incubated at 37°C for 0 min or 90 min before processing for in situ hybridization. For detection of the viral replication centers, A549 cells were incubated with 250 ng EdA/EdC-HAdV-C5 at 37°C for 60 min. The virus inoculum was removed and samples further incubated at 37°C for 16 h before processing for in situ hybridization.

Supplemental References

Davis, L.I., and Blobel, G. (1987). Nuclear pore complex contains a family of glycoproteins that includes p62: glycosylation through a previously unidentified cellular pathway. Proc Natl Acad Sci USA *84*, 7552-7556.

Deppert, W., Walser, A., and Klockmann, U. (1988). A subclass of the adenovirus 72K DNA binding protein specifically associating with the cytoskeletal framework of the plasma membrane. Virology *165*, 457-468.

Greber, U.F., Suomalainen, M., Stidwill, R.P., Boucke, K., Ebersold, M., and Helenius, A. (1997). The role of the nuclear pore complex in adenovirus DNA entry. EMBO J *16*, 5998-6007.

Varghese, R., Mikyas, Y., Stewart, P.L., and Ralston, R. (2004). Postentry neutralization of adenovirus type 5 by an antihexon antibody. J Virol *78*, 12320-12332.

Walkiewicz, M.P., Morral, N., and Engel, D.A. (2009). Accurate single-day titration of adenovirus vectors based on equivalence of protein VII nuclear dots and infectious particles. J Virol Methods *159*, 251-258.